PRECIPITATION ON SUBSTRUCTURE IN IRON-BASE ALLOYS

A. S. Keh, W. C. Leslie and G. R. Speich
Edgar C. Bain Laboratory for Fundamental Research
United States Steel Corporation Research Center
Monroeville, Pennsylvania

Abstract

An attempt is made to summarize the current state of knowledge of precipitation on defects in iron-base alloys, and the effect of precipitation on the properties of such alloys.

1. Introduction

The development and nature of substructure in metals and alloys have been described in several of the foregoing papers in this symposium. The effects of substructure on mechanical properties and recrystallization behavior have been discussed. As metallurgists, we are interested in understanding and employing as many different techniques as possible to control and improve the properties of engineering alloys. It is obvious, then, that we should consider the advantages to be gained by combining the effects produced by substructure and by precipitation from solid solution. Our understanding of these combined effects has been vastly improved in recent years by use of transmission electron microscopy, which allows us to study the details of precipitation on substructure.

Iron-base alloys are of particular interest, not only because of their paramount importance as engineering materials, but also because of the large number of possible combinations of defect structures and precipitates that exist. In cold-worked ferrite, the substructure can consist of dislocations clustered into cell walls, or of a uniform distribution of dislocations and some deformation twins. After annealing, the substructure can consist of low-angle boundaries. Cold-worked austenitic alloys can contain all the arrangements of defects that are possible in cold-worked ferrite, with the addition of stacking faults. The most complicated defect structures are those which result from the transformation from austenite to ferrite. If the rate of cooling is fairly slow, as after hot rolling, the resulting ferrite contains low-angle subboundaries. If the rate of cooling is high, as in a quench, or if the composition of the alloy is adjusted to produce a low Ms temperature, the resulting ferrite has a martensitic structure, containing a very high density of dislocations, closely-spaced boundaries produced by shear, and frequently, very fine twins within martensite plates. The purpose of this paper is to show how precipitation from solid solution is affected by substructure in ferritic, austenitic and martensitic alloys. Several examples will be cited of the use of precipitation on substructure to improve the properties of alloys.

Although research into the details of these processes is quite recent, a great deal of information is being developed very rapidly, so the authors hope they will be forgiven if they have overlooked any contributions.

2. Theory of Nucleation on Dislocations

According to the classical theory of nucleation, the total free energy change, ΔF, accompanying the formation of a nucleus of a second phase from a supersaturated solid solution can be expressed by

$$\Delta F = \Delta F_{volume} + \Delta F_{surface} + \Delta F_{strain} \cdots \qquad (1)$$

The change in volume free energy must be negative. The changes in surface free energy, $\Delta F_{surface}$, and strain free energy, ΔF_{strain}, due to formation of the nucleus, are positive. The total change of free energy is positive and increases to a maximum up to a critical size of the nucleus. When the radius of the nucleus exceeds the critical value, r_o, ΔF begins to decrease and the nucleus will then be stable.

The activation energy for precipitation is less at a dislocation than in the perfect lattice. Cahn (1) has developed a theoretical treatment of nucleation on dislocations. Assuming a cylindrical, noncoherent nucleus of radius r lying along a dislocation, he associated the strain energy of the dislocation with the strain energy required for nucleation, to reduce the barrier to nucleation. According to his treatment, the free energy per unit length of dislocation occupied by the nucleus can be expressed by

$$F = -A \log r + 2\pi \gamma r - \pi \Delta F_{volume} r^2 + C \qquad (2)$$

where

$$A = \frac{Gb^2}{4\pi(1-\nu)} \text{ for an edge dislocation}$$

$$= \frac{Gb^2}{4\pi} \text{ for a screw dislocation}$$

G = shear modulus

b = Burgers vector

ν = Poisson's ratio

γ = interfacial energy of the boundary

A minimum in free energy was found when the quantity

$$\alpha = \frac{2A \Delta F_{volume}}{\pi \gamma^2} < 1$$

This circumstance, which is analogous to the presence of a Cottrell atmosphere, is indicated schematically in Fig. 1, at A. In Cahn's model, the free energy can then increase with increasing radius of the nucleus. If the quantity $\alpha > 1$, i.e., if supersaturation is higher, this barrier can disappear, and the precipitate can nucleate and grow at a rate limited only by diffusion. Cahn's model predicts that dislocations become more effective catalysts for nucleation, relative to homogeneous nucleation, with increasing temperature and increasing supersaturation. The temperature and concentration dependence of the nucleation energy is greater at dislocations than for homogeneous nucleation.

Since Cahn's paper was written, the physical situations existing during precipitation have been found to be so complex (2) that his relatively simple model cannot be expected to correspond to many of the observations. In our own observations, for example, it has been found that the temperature and concentration dependence of matrix nucleation is greater than for dislocation nucleation.

3. Precipitation on Dislocations and Subboundaries in Ferritic Alloys

3.1 Precipitation of Interstitial Solutes

With the advent of transmission electron microscopy, precipitation in Fe-C and Fe-N alloys has been investigated extensively in several laboratories (3-8), and the effects of dislocations and subboundaries on the kinetics and morphology of precipitation have become evident. In general, dislocations are preferred sites for precipitation of carbides and nitrides in iron, but grain boundaries are preferred at high aging temperatures (low supersaturation) and matrix nucleation occurs at low aging temperatures (high supersaturation). Because of uncertainty as to the nature of the matrix sites, the term "homogeneous nucleation" will not be used. The exact mode of precipitation is critically dependent upon solute concentration, aging temperature, and dislocation density.

In both Fe-C and Fe-N alloys, a metastable phase is precipitated at low aging temperatures. In common with nearly all low-temperature precipitates in cubic metals, the particles form as disks on $\{100\}_\alpha$ planes, the disks being the configuration of minimum strain energy and $\langle 100\rangle_\alpha$ being the directions of minimum modulus of elasticity (2). These phases are not affected by the nucleation site; they are the same whether formed on dislocations or in the matrix. Most investigators have concluded that the low-temperature carbide is the hexagonal ε (7,9,10) but there remains a possibility that it may have a body-centered tetragonal structure, analogous to the structure of the α'' nitride, $Fe_{16}N_2$ (3,11). At higher aging temperatures, cementite, Fe_3C, is formed. It appears as dendrites on $\{110\}_\alpha$, with the branches growing in $\langle 111\rangle_\alpha$ (12,13). Both carbides nucleate preferentially on dislocations, although they also nucleate on unidentified matrix sites, at high supersaturation.

In the iron-nitrogen system, there appears to be no doubt of the identification of the metastable nitride precipitated from ferrite at low aging temperatures; it is the α'' phase, $Fe_{16}N_2$ (5,14,15). The γ' phase, Fe_4N, precipitated at higher temperatures, is face-centered cubic. It can nucleate at dislocations or at grain boundaries.

It is worth repeating that in both the Fe-C and Fe-N systems, the structure of the precipitate is not affected by the nucleation site. This is not necessarily true in other systems; for example, in some aluminum alloys where a sequence of precipitation occurs, the microstructure consists of GP zones in the matrix and an intermediate phase on the dislocations (2).

If the dislocation density is not very high ($\lesssim 10^8/cm^2$), and if the aging temperature is low, uniform matrix precipitation is observed, in addition to precipitation on dislocations. At higher aging temperatures, the supersaturation of the same alloy is less, and precipitates form exclusively on dislocations. Fig. 2 illustrates these differences in an Fe-0.02 wt.% N alloy, aged at 100° and at 200°C. If the dislocation density in an Fe-N alloy is high ($> 10^9/cm^2$), precipitation on dislocations

predominates, but the details of precipitation change with aging temperature. At low aging temperatures, precipitation occurs on all dislocation segments, irrespective of dislocation orientation. The precipitates thus formed are dendritic (Fig. 3a). In the same alloy aged at higher temperatures, precipitates form only on dislocations lying on $\{100\}_\alpha$, the habit plane of the precipitate (Fig. 3b). This difference is presumed to be due to the difference in chemical driving force. At the higher aging temperature, ΔF_{volume} in Eq. 1 is smaller, and dislocations must be favorably oriented for their strain energy to suffice for nucleation. At the lower temperature, the nitrogen atoms segregate to all dislocations, and since the chemical driving force is higher, precipitation occurs even on dislocations not lying on $\{100\}_\alpha$. In this circumstance, jogs probably first form on $\{100\}_\alpha$, then nitride particles grow from these jogs.

Dislocation orientation has a definite effect on the precipitation of carbides and nitrides in alpha iron. On pure screw dislocations, the precipitate can form as a spiral (Fig. 4). The alloy illustrated is Fe-0.45% Mn-0.017% C, quenched from 720°C, then aged 1 hour at 100°C. The plane of the foil is $\{110\}$ and the directions of the dislocations are $[1\bar{1}1]$ and $[1\bar{1}\bar{1}]$. It is well known that screw dislocations can be converted to helices by vacancy condensation. Such helices have not been observed in quenched, high-purity iron. Their presence in the Fe-Mn-C alloy suggests that the substitutional or interstitial solute atoms inhibit the annealing-out of vacancies, which then congregate at screw dislocations, prior to precipitation.

Precipitation can occur preferentially on one side of edge dislocations. Fig. 5 shows a simple tilt boundary, decorated with a precipitate of $Fe_{16}N_2$. It was not established whether the precipitates form on the tension or on the compression side of the dislocations. They would be expected to form on the tension side if vacancies were not involved in the precipitation process. In either case, precipitation should be confined to one of the three $\{100\}$ planes, which is what is observed in Fig. 5. The subboundary illustrated also contains a few "foreign" dislocations, which intersect and interact with the edge dislocations, forming short segments at the points of intersection. The mode of precipitation on these "foreign" dislocations and short dislocation segments differs from that on the edge dislocations.

Some dislocations on subboundaries are more favorable sites for precipitation than others. Precipitation in an Fe-3% Si-0.01% C alloy seemed to favor the [100] segments of the dislocation network formed by the reaction $a/2\,[111] + a/2\,[1\bar{1}\bar{1}] \rightarrow a[100]$, (Fig. 6). In Fig. 7, precipitation on one set of dislocations in the subboundary has a stepwise appearance and appears very dark, whereas the precipitate on the horizontal parallel set of dislocations is much lighter in shade. The zigzag dislocations are believed to be a metastable configuration formed by a dislocation interaction, as shown schematically in Fig. 7.

3.2 Precipitation of Substitutional Solutes

In a sustained effort to determine the important factors governing the precipitation of substitutional solutes from ferrite, studies have been made of the binary alloys of iron with copper and gold (16), titanium and niobium (17) and phosphorus (18). Nucleation in an alloy containing 1.1 atom per cent copper, aged at temperatures from 500 to 700°C after quenching from 840°C, was compared with nucleation in an alloy containing 1.1 atom per cent gold, similarly treated. The precipitating phase in both instances is face-centered cubic, being a dilute solution of iron in copper or in gold. In the Fe-Au alloy, nucleation occurred exclusively on dislocations and subboundaries, (Fig. 8), but in the Fe-Cu alloy, nucleation was general (Fig. 9). Hornbogen(16) attributed this difference to the difference in atomic size of the solute atoms. The copper atom is nearly the same size as the iron atom, and the atomic volumes of matrix and precipitate are almost identical. Little strain energy should be required for nucleation of the copper-rich phase. On the other hand, the gold atom is much larger than the iron atom ($r_{Au}/r_{Fe} = 1.13$) and the atomic volume of the precipitate is much greater than that of iron. In the precipitation of copper, almost the only barrier to be overcome is the surface energy. To nucleate a particle of gold, however, a large strain energy barrier must be overcome, in addition to the surface energy, so the core energy of dislocations must be utilized. Precipitation tends to be confined to dislocations and subboundaries. This conclusion of the predominant effect of solute atom size on selection of nucleation site, based as it is on one solute concentration, would be strengthened by similar studies made with other concentrations. As will be shown later, copper precipitates can be restricted to dislocations when the supersaturation is lower.

Hornbogen proposed that nucleation of gold-rich particles on dislocations occurs in several steps:

1. Segregation of gold atoms to dislocations.
2. Formation of stacking faults on $\{100\}_\alpha$ by the reaction

$$\frac{a}{2}[111] \rightarrow \frac{a}{2}[110] + \frac{a}{2}[001].$$

3. Segregation of gold to the stacking fault.

The a/2 [110] dislocation is glissile and can move as fast as gold atoms can segregate into the stacking fault. The a/2 [001] dislocation is sessile and remains in its original position as the stacking fault grows.

Speich (17) has found that dislocations and grain boundaries in ferrite are preferred sites for nucleation in Fe-Ti and Fe-Nb alloys. The precipitates are the $MgZn_2$ type Laves phases Fe_2Ti and Fe_2Nb, respectively.

Precipitation in the Fe-P system shows some interesting differences from the examples discussed previously. To obtain a high degree of supersaturation and a controlled density of dislocations, Hornbogen (18) quenched

a ferritic Fe-1.8% P alloy from 1100°C, immediately after hot rolling. The sequence of precipitation during subsequent aging at 500°C is shown in Fig. 10. The as-quenched specimen contained subboundaries and isolated dislocations (Fig. 10a). Precipitates began to form at dislocation intersections (Fig. 10b) after 4 hours at 500°C. Considerable growth had occurred after 10 hours' aging (Fig. 10c). Only after 54 hours' aging at 500°C did nucleation occur in the matrix, and then the particles differed from those formed on dislocations, being rods instead of plates. The rods grew on $\{100\}_\alpha$ in $\langle 012\rangle_\alpha$ directions.

It is a general observation (3,6,18) that precipitate particles nucleated on dislocation networks (subboundaries) do not grow to be as large as those nucleated on isolated dislocations or in the matrix. When nucleation sites are closely spaced, as in a subboundary, the volume from which a growing particle can draw solute atoms is severely limited, and growth soon stops. This limitation is not imposed on particles growing on isolated dislocations, or in the matrix. This effect is illustrated in Fig. 11.

Studies of rates of growth of precipitate particles are complicated by the general finding (3,16,19) that not all nuclei grow until the matrix has reached the equilibrium concentration of solute. Growth of larger particles occurs at the expense of smaller ones, long before the matrix is depleted of solute. A particle on an isolated dislocation can grow at the expense of smaller particles in a subboundary, or in the matrix.

It has also been found (3,18) that the temperature dependence of matrix nucleation is greater than that of dislocation nucleation. This effect, in an Fe-1.8% P alloy, is illustrated in Fig. 12. Matrix nucleation is favored by decreasing temperature, i.e., increasing supersaturation. By extrapolation of the lines in Fig. 12, matrix and dislocation nucleation of phosphides would be simultaneous at about 350°C.

4. Precipitation on Substructure in Austenitic Alloys

4.1 Precipitation on Dislocations

The factors which influence precipitation on dislocations in ferrite also affect precipitation on dislocations in austenite. The size effect discussed in Section 3.2 is apparently involved in some interesting observations made by Irani and Honeycombe (20) on precipitation of carbides on dislocations in retained austenite in Fe-4% Mo-02% C and Fe-1% V-0.2% C alloys. Specimens were quenched, then tempered at 500 and 700°C. In the Fe-Mo-C alloy tempered at 500°C helical dislocations were formed very similar in appearance to those illustrated in Fig. 4 of this paper. Additional tempering caused the formation on dislocations of a very fine precipitate, which later became recognizable as Mo_2C. On the other hand, dislocations did not play a major role in precipitation of carbides in the Fe-V-C alloy. These carbides appeared to form in the matrix from zones rich in vanadium and carbon. At least part of the difference in precipitation was attributed to the difference in atomic diameter between

molybdenum and vanadium. The larger molybdenum atom would tend more to segregate at dislocations than would the atoms of vanadium. Also, nuclei of molybdenum carbide would be less easily accommodated in the perfect lattice than would nuclei of vanadium carbide, which has a smaller unit cell. The net effect on nucleation is analogous to the differences in the precipitation of copper and gold from alpha iron.

Dislocations can be generated around large, undissolved carbide particles in austenite, or in ferrite, during the cooling of the steel, because of the stresses generated by contraction of the matrix around the particle. Such dislocation networks can serve as nucleation sites for precipitation during subsequent aging (17,21).

4.2 Precipitation on Twin Boundaries in Austenitic Alloys

Hatwell and Berghezan (22) employed a Type 316 stainless steel in a study of precipitation of $M_{23}C_6$ carbides at the boundaries of annealing twins in austenite. If the specimens are carefully handled during the solution and aging treatments, the twin boundaries remain coherent and are not preferred sites for precipitation. However, if the quench is drastic, or if the specimen is strained plastically prior to aging, dislocations pile up at the twin boundaries, i.e., coherency is lost, and these boundaries then become preferred sites for precipitation. The shape of the precipitated carbide in this instance depended upon the nucleation site; at grain boundaries the carbides were dendritic, whereas at the twin boundaries the precipitate particles were triangular, growing on $\{111\}_\gamma$ planes.

It should be noted here that the boundaries of mechanical twins in ferritic alloys always contain a high density of dislocations; matrix-mechanical twin boundaries are never coherent, so they should provide an abundance of nucleation sites for precipitation.

4.3 Precipitation on Stacking Faults in Austenitic Alloys

It was first pointed out by Suzuki (23) that solute atoms can segregate to stacking faults and thereby lower the stacking fault energy. Hendrickson (24), using the data of Howie and Swann (25), and Suzuki (26) have recently calculated the extent of such segregation. Once segregation has occurred, precipitation at the stacking fault will be favored because of the reduction of the surface energy term, $\Delta F_{surface}$, in Eq. 1. Nicholson (27) has shown that stacking faults in an Al-7% Mg alloy can act as nucleation sites for an hexagonal precipitate. More recently, van Aswegen and Honeycombe (28) have observed the precipitation of NbC on stacking faults in an 18% Cr-10% Ni-1% Nb austenitic stainless steel. After quenching from 1300°C, precipitation of NbC occurred during tempering in the range 650° to 850°C. Dislocations in the as-quenched alloy were not dissociated. Stacking faults began to appear after 5 hours at 700°C, and longer periods at this temperature resulted in formation of NbC, as shown in Fig. 13. The precipitation of the carbide at the stacking faults was attributed to the prior segregation of niobium atoms. Tempering above and below the 650°-

850°C range led to precipitation of NbC on undissociated dislocations, but the maximum strengthening corresponded to the onset of precipitation on stacking faults.

Similar observations on stacking fault precipitation in the same alloy were made by Pickering, Burns and Keown (29). They determined that the faults lie on $\{111\}_\gamma$, and the orientation relationship is $\{100\}_{NbC} \| \{100\}_\gamma$ and $\langle 100\rangle_{NbC} \| \langle 100\rangle_\gamma$.

5. Precipitation on Transformation Substructure

5.1 Types of Transformation Substructure

Kelly and Nutting (30,31) found principally two types of transformation substructure in iron-base alloys. The first type, characteristic of high-carbon martensites, consisted of internally twinned plates. This is illustrated by the microstructure of a quenched 1.0% C steel (Fig. 14). The twins, which are parallel to $\{112\}_M$, are about 100 Å thick and irregularly spaced. These internal twins evidently arise from the need for an inhomogeneous "second" shear accompanied by a "first" shear which is homogeneous on a macroscopic scale, to generate the martensite lattice from the austenite. The internal twins constitute this "second" inhomogeneous shear. The internally twinned plates have also been observed (30,31) in quenched 0.4 and 0.8% C steels, in martensite formed at -95° and -196°C in an Fe-20% Ni-0.8% C steel, and in Fe-30% Ni alloys by Nishiyama and Shimizu (32,33) and Warlimont (34).

The second type of transformation substructure is characteristic of quenched martensites in low-carbon steels and in 18-8 stainless steel. It consists of martensite needles with no internal twinning but with a very high dislocation density. An example from a 0.1% C steel is shown in Fig. 15. The long axis of the needles is parallel to $\langle 111\rangle_M$. As the carbon content of the martensite is increased there is an increasing tendency for the needles to be grouped together in the form of "sheets". The orientation difference between needles in the "sheet" is usually only a few degrees although in some cases they seem to be twin related. This type of transformation substructure is also characteristic of martensite formed in Fe-30% Ni alloys and in other alloys of similar nickel content, such as the maraging steels (35). An example of the structure of an Fe-30% Ni martensite is shown in Fig. 16.

The transition from needles with a very high dislocation density in a 0.1% C steel to internally twinned plates in a 1.0% C steel occurs gradually as the carbon content is increased. Intermediate carbon contents contain mixtures of both types. Kelly and Nutting (31) postulated that the two factors controlling the type of transformation substructure are the transformation temperature and the stacking fault energy, with the composition of the steel only affecting the substructure through its effect on these two parameters. High Ms temperatures and low stacking fault energies favor the formation of martensite needles, whereas low Ms temperatures and high stacking fault energies favor the formation of internally twinned plates.

5.2 Tempering of Iron-Carbon Martensites

Kelly and Nutting (30,31) examined the structural changes during the

tempering of 0.14 and 1.0% C steels and Turkalo (36) has studied the tempering behavior of a 0.42% C steel. In the 0.14% C steel, auto-tempering occurred during quenching and Widmanstätten carbides in the form of plates or laths about 100 Å wide and 1500 Å long were visible in about 10% of the grains in the as-quenched structure. After tempering at 300°C, carbide particles were visible in all grains. Further tempering increased the thickness of the carbides.

In the 0.42% C steel studied by Turkalo (36), the primary substructure appeared to be martensite needles with a high dislocation density, although some internal twinning was evident. Although Turkalo indicated that the twins were within the "needles", the structure may actually be a mixture of internally twinned plates and twin-free martensite needles, as Kelly and Nutting (30) found in a 0.4% C steel. On tempering at 205°C carbide films appeared at the martensite needle boundaries. After tempering at 315°C, two types of carbides appeared within the grains--"streaky" carbides and "crystallographic" carbides which formed in two directions in the martensite. The latter carbides appear to be parallel to $\{110\}_\alpha$. Examples of both types are shown in Fig. 17. The carbide films at the martensite needle boundaries become thicker and less continuous at higher tempering temperatures. With further increases in tempering temperature, spheroidization of the carbides occurred, along with the formation of subboundaries in the ferrite, and eventually, recrystallization of the ferrite. The structure after tempering at 595°C consisted of fine ferrite grains and spheroidized carbides.

In 1.0% C steel the primary substructural feature that influences precipitation appears to be the internal twins (30,31). Tempering at 200°C resulted in the appearance of carbides lying along the twins in the martensite, together with tiny precipitates perpendicular to the twin plane. These small precipitates disappeared after tempering at 300°C, whereas the lath-like carbides lying along the twins became more prominent (Fig. 18).

These latter carbides were identified as cementite, with the orientation relationship:

$$(211)_\alpha \| (001)_{Fe_3C}$$

$$[0\bar{1}1]_\alpha \| [100]_{Fe_3C}$$

$$[1\bar{1}1]_\alpha \| [010]_{Fe_3C}$$

The small precipitates formed normal to the twin plane are believed to be ε carbide, although the diffraction patterns obtained by Kelly and Nutting (31) were not sufficient to allow identification.

5.3 Precipitation from Substitutional Martensites

Recently, much attention has been focused on precipitation from substitutional martensites, principally because of development of precipitation hardening stainless steels (37) and "maraging" steels (38). The structure of the martensite in these alloys is of the same type shown

in Fig. 16 for an Fe-20% Ni alloy. The martensite "needles" contain a very high density of dislocations, but no internal twins. The substructural features affecting precipitation are the boundaries between the needles and the dislocations within the needles. A polygonized substructure can be formed by recovery of the transformation substructure itself, as shown in Fig. 19 for an Fe-18% Ni-7% Co alloy aged 100 hrs. at 500°C. In this alloy no precipitation occurred since it was aged in an $\alpha + \gamma$ region.

Another process that may occur during precipitation in substitutional martensitic alloys is the formation of austenite, since the alloys are generally aged at a temperature at which austenite is stable. The structure of an Fe-20% Ni alloy aged in the $\alpha + \gamma$ region for 100 hrs. at 500°C is shown in Fig. 20. X-ray diffraction indicated that the specimen contained 40% austenite after this treatment. The extinction fringes are believed to outline the thin films of austenite, which appear to form in the martensite needle boundaries; thus, the sites for austenite formation may be controlled by the original transformation substructure. In alloys in which an intermetallic compound precipitates, recovery of the transformation substructure and formation of austenite may be occurring simultaneously with precipitation.

The precipitation of intermetallic compounds from martensitic alloys is affected principally by the dislocations within the martensite needles. Fig. 21 shows the very fine dispersion of Ni_3Ti particles that forms on aging of an Fe-20% Ni-1% Ti alloy. Fig. 22 is an example of precipitation of copper in an Fe-20% Ni-10.7% Cu alloy. Fig. 23 shows precipitation in an Fe-18% Ni-7% Co-5% Mo alloy, which has nearly the same composition as some maraging steels, but without titanium. In all three instances the precipitate occurs in an extremely fine dispersion as a result of the high density of dislocations giving a high density of nucleation sites.

6. Effects and Applications of Precipitation on Substructure

6.1 The Role of Substructure in Quench-Aging and Strain-Aging of Iron and Steel

It has been demonstrated (3,6,19) that the strengthening associated with quench-aging in Fe-C and Fe-N alloys and in commercial low-carbon steels, depends upon a uniform dispersion of fine precipitated particles in the matrix. If precipitation is restricted to the dislocations present before aging, an uneven dispersion of relatively coarse particles results, and the interparticle spacing is uaually too great for effective strengthening.

In contrast to quench aging, strain aging in iron and steels is strongly dependent upon interactions between interstitial solute atoms and the dislocations introduced before or during the aging treatment. A question frequently arises as to whether the strengthening associated with strain-aging is due to segregation of interstitial atoms to dislocations, to the actual formation of precipitates at dislocations, or both. According to Cottrell and Bilby (39) the dislocations should be saturated when the concentration of interstitial solutes reaches one atom per atom plane per dislocation line. Later experiments, especially those employing internal friction to determine the kinetics of precipitation, suggest a higher degree of segregation (40-42). These results suggested that precipitation, as well as segregation, occurred during strain aging. Wilson and Russell (43), using a replica technique,

showed some evidence of precipitation during strain aging. The Cottrell-Bilby theory has been modified by Bullough and Newman (44) to accommodate precipitation.

By means of transmission electron microscopy, Leslie and Keh (45) have shown that precipitation need not necessarily occur during strain aging. In an Fe-C alloy, slowly cooled from the annealing temperature, and in an Fe-N alloy quench-aged at a very low temperature then strained and aged, no additional precipitates were observed on dislocations, although there was a return of the yield point, and a sharp upward shift in the flow curves. The structures prior to strain aging consisted of ferrite and large carbide or small nitride particles. During straining and aging, a small fraction of the carbon and nitrogen probably re-dissolved and segregated along dislocation lines. However, in these circumstances, it is quite impossible for new particles to form. As pointed out by Kelly and Nicholson (2), a precipitate on a dislocation is not in a lower energy state than one of the same type in the matrix, and there can be no tendency for the former to grow while the latter dissolves.

On the other hand, if one starts with Fe-C or Fe-N, or with a low-carbon steel, in the condition of a supersaturated solid solution, then strains and ages the specimens, precipitation on dislocations will occur in the later stages of aging. This is superposing quench aging upon strain aging. Fig. 24 illustrates the aging of an Fe-0.02% N alloy, quenched from 500°C, then strained 3% in tension. After one minute at 100°C, no precipitates could be seen on the dislocations introduced during prestraining; however, an appreciable amount of strain aging had occurred. The strain aging index continued to increase with aging time, reaching a plateau after 10 minutes. At this point, the first fine precipitates were observed on dislocations. As aging proceeded, the alloy continued to strengthen. The precipitates on dislocations continued to grow, and particles began to form in the matrix as shown in Fig. 25a. After two hours at 100°C, the strain aging index reached a maximum. As aging progressed, the nitride particles agglomerated, freeing some dislocation segments (Fig. 25b). This change in structure was accompanied by a decrease of the strain aging index. It should be noted here that the first particles seen on dislocations are discrete platelets, lying on $\{100\}_\alpha$, with a diameter of about 30 Å. This observation differs from the theory of Bullough and Newman (44), who deduced a continuous particle, lying along the dislocation line.

The strain aging of steels is usually considered to have undesirable consequences in the way of reduced ductility, embrittlement and surface flaws, but overemphasis of these effects can serve to obscure the fact that strain aging can be an economical means of raising the strength level. The recent interest in warm-working of steels is a case in point (46). When steels are worked in the temperature range between 150 and 350°C, aging occurs simultaneously with straining. The rate of work-hardening is much greater than during straining at room temperature. It has been found (19) that the dislocation density after straining a low-carbon steel 3% at 200°C is about five times higher than in the same steel strained 4% at room temperature. This evidence supports the proposal (45) that dislocations strongly pinned during strain aging are not freed from their atmospheres, but that straining proceeds by the generation of new dislocations.

6.2 Control of Recrystallization by Precipitation on Substructure

Precipitation on substructure can be used, in a practical sense, to control the structure and properties of alloys. One such instance is the use of precipitation on substructure in a cold-worked metal to control the kinetics of recrystallization, and the grain size and shape, texture and mechanical properties in the annealed, recrystallized condition. The process depends upon solution of an alloying element or compound in the alloy. This may occur during hot rolling. Following the solution treatment, the alloy is cooled rapidly to retain the solutes in supersaturated solid solution, then cold worked and annealed. By suitable control of the annealing cycle, precipitates can be nucleated at subboundaries (cell walls) before the cells have grown to form recrystallized grains. Nucleation of such precipitates stabilizes the cell structure, greatly decreasing the number of cells which can grow, thereby decreasing the overall rate of recrystallization, and producing fewer and larger recrystallized grains.

Commercially, the most important application of this process is in the production of low-carbon, aluminum-killed sheet steels for applications involving severe forming. The precipitate in this instance is aluminum nitride. Fig. 26, taken from Rickett, et al (47), illustrates the drastic change in recrystallization kinetics that results from the precipitation of this compound during the annealing of cold-rolled low-carbon steel. The phenomenon does not depend upon precipitation of aluminum nitride alone, however. The following examples are taken from a dilute alloy of copper in iron (48). Fig. 27 illustrates the differences in structure produced in iron by precipitation during the process of recrystallization. In the high-purity iron, the recrystallized grains are nearly equiaxed. In the dilute Fe-Cu alloy, the grains are much larger and are in the shape of pancakes, with their diameter being about four times their thickness. This is the type of ferrite structure which gives aluminum-killed, low-carbon sheet steel its optimum drawing properties. The stepped annealing treatment of 3 hours at 500°C, followed by 5 hours at 700°C, initiates precipitation on the cell walls in the cold-worked alloy, then completes the process of recrystallization.

To obtain this structure of elongated recrystallized grains two factors are necessary:

1. A decrease in the number of "nuclei" for recrystallization, i.e. a decrease in the number of cells which grow to become recrystallized grains. Fewer "nuclei" results in fewer and larger recrystallized grains.

2. Barriers at the boundaries of cold-worked grains which prevent the new recrystallized grains from growing across these boundaries. The recrystallized grains tend to conform to the shape of the prior cold-worked grains.

Both factors are present when precipitation occurs preferentially on cell walls and on grain boundaries. Fig. 28, taken from Leslie, et al (49), shows preferential precipitation of copper in cell walls, which is effective in preventing migration of these walls, i.e., recrystallization is strongly inhibited. This preferential precipitation occurs despite the

fact that, as discussed in Section 3.2, there is not a strong elastic interaction between copper atoms and dislocations in iron. The effect might be even more pronounced if there were a large size difference between the iron and the solute atoms.

Fig. 29 shows the other requirement for the elongated grain ferrite structure, precipitation in grain boundaries. The growth of the few cells which do break away from the contraint of the precipitate particles in cell walls is stopped at the grain boundaries. Thus, only one of two grains may be nucleated within each prior cold-worked grain, and these grow principally within the bounds of the cold-worked grain, giving the pronounced elongation shown in Fig. 27.

Precipitation occurring after cold rolling, but before recrystallization, can also be used to control texture. The precipitation of copper in cold-rolled iron, for example, tends to increase the retention of the cold-worked texture after annealing and prevents the formation of the usual annealing texture (48).

This procedure of controlling microstructure and texture by preferential precipitation on substructure should be applicable to many metallic systems (e.g. iron in aluminum, "doped" tungsten), but to date it has not been consciously exploited to any great extent. Increased application may follow improved understanding of the process.

6.3 Use of Substructure to Reduce Grain Boundary Embrittlement

In systems wherein grain boundary embrittlement due to segregation of solutes is a problem, ductility can be improved by introducing substructure, which serves to decrease the concentration of solute at the grain boundaries. For example, it is impossible to quench an iron-1.8% phosphorus alloy from high temperatures without producing intergranular cracks (50). However, if the alloy is hot-worked immediately before quenching, the cracks are eliminated and the alloys can subsequently withstand slight plastic deformation at room temperature. The density of substructure introduced by hot rolling is illustrated in Fig. 30. After hot rolling to 80% reduction in thickness at 1100°C, the high angle grain boundaries are not visible in the welter of dislocations.

6.4 Reduction of Creep Rate by Precipitation on Substructure in Austenite

A fourth example of the practical value of precipitation on substructure is the improvement of the creep characteristics of Type 316 austenitic stainless steel developed by prestraining at room temperature, followed by aging at 480° then at 705°C (51). This pretreatment leads to the precipitation of $M_{23}C_6$ carbides at dislocation sites. In the absence of prestrain, creep testing at 705°C results in the precipitation of coarse carbides at grain boundaries. For a testing temperature of 705°C, the minimum creep rate decreases and the rupture life increases as the prestrain is increased up to 25 or 30%. At these levels of prestrain, most of the dislocations are present in broad deformation bands. Precipitation within these bands, as shown in Fig. 31, is much more effective in decreasing the minimum creep rate than is a general dispersion of particles. A pretreatment of 24 hours at 480°C and 216 hours at 705°C decreases the minimum creep rate by a factor

of 250 and increases the rupture life by a factor of 10 during creep testing at 705°C.

Hatwell and Berghezan (22), who also employed Type 316 stainless, found precipitation within grains only after 20% plastic strain. The difference between their results and those of Garofalo, et al (51), is almost certainly due to the two-stage aging treatment used by the latter. The initial treatment at 480°C nucleated carbides at dislocations and the subsequent treatment at 705°C allowed these to grow. Hatwell and Berghezan aged their specimens at 750°C after plastic deformation, a temperature too high for nucleation on dislocations, unless the dislocation density is quite high.

Irvine, Murray and Pickering (52) have shown that precipitation on dislocations and subboundaries in an austenitic stainless steel can be controlled by warm-working, as an alternative to the straining and aging sequence employed by Garofalo, et al (51), and by Hatwell and Berghezan (52).

Acknowledgment

The authors wish to thank F. W. Aul, R. C. Glenn, R. L. Miller, C. M. Owens, R. D. Schoone, and D. W. Stevens, of the staff of the Edgar C. Bain Laboratory, for their assistance in these investigations. Much of the work was carried out by E. Hornbogen, who has made substantial contributions to our knowledge in this field. The consistent encouragement of R. L. Rickett over a period of years has been of great help in the continuation of these studies.

References

1. J. W. Cahn, Acta Met. 5, 169 (1956).

2. A. Kelly and R. B. Nicholson, to be published, Progress in Materials Science, Academic Press, N.Y.

3. W. C. Leslie, Acta Met. 9, 1004 (1961).

4. E. Smith, Direct Observations of Imperfections in Crystals, Interscience, N.Y., 1962, p.203.

5. W. Pitsch, Arch. Eisenhuttenw. 32, 493 (1961).

6. A. S. Keh and H. A. Wriedt, Trans. AIME 224, 560 (1962).

7. K. F. Hale and D. McLean, to be published.

8. D. Hull and I. L. Mogford, Phil. Mag., 6, 535 (1961).

9. W. Pitsch and A. Schrader, Arch. Eisenhuttenw. 29, 715 (1958).

10. A. L. Tsou, J. Nutting and J. W. Menter, J. Iron Steel Inst. 172, 163 (1952).

11. R. H. Doremus and E. F. Koch, Trans. AIME 218, 591 (1960).

12. W. C. Leslie, R. M. Fisher and N. Sen, Acta Met. 7, 132 (1959).

13. W. Pitsch and A. Schrader, Arch. Eisenhuttenw. 29, 485 (1958).

14. K. H. Jack and D. Maxwell, J. Iron and Steel Inst. 170, 254 (1952).

15. G. R. Booker, J. Norbury and A. L. Sutton, Ibid. 187, 205 (1957).

16. E. Hornbogen, Acta Met. 10, 525 (1962).

17. G. R. Speich, Trans. AIME 224, 850 (1962).

18. E. Hornbogen, to be published, Trans. ASM.

19. A. S. Keh and W. C. Leslie, to be published, Structure and Properties of Engineering Materials, John Wiley and Sons, N.Y.

20. J. J. Irani and R. W. K. Honeycombe, 5th Inter. Con. for Electron Micros., Academic Press, N.Y., 1962, 1, p.HH-9.

21. J. Nutting and J. M. Arrowsmith, Iron Steel Inst. Spec. Report No. 70, 1961, p.147.

22. A. H. Hatwell and A. Berghezan, Iron Steel Inst. Spec. Report No. 64, 1959, p.88.

23. H. Suzuki, Sci. Rep. Res. Inst. Tohoku Univ. A1, 183 (1949).

24. A. A. Hendrickson, Acta Met. 10, 900 (1962).

25. A. Howie and P. R. Swann, Phil. Mag. 6, 1215 (1961).

26. H. Suzuki, J. Phys. Soc. Japan 17, 322 (1962).

27. R. B. Nicholson, to be published, Electron Microscopy and Strength of Crystals, John Wiley and Sons, N.Y.

28. J. S. T. van Aswegen and R. W. K. Honeycombe, Acta Met. 10, 262 (1962).

29. F. B. Pickering, K. W. Burns and S. R. Keown, 5th Int. Cong. Electron Micros. Academic Press, N.Y., 1962, 1, p.CC-4.

30. P. M. Kelly and J. Nutting, Proc. Roy. Soc. 259, 45 (1960).

31. P. M. Kelly and J. Nutting, J. Iron Steel Inst. 197, 199 (1961).

32. Z. Nishiyama and K. Shimizu, Acta Met. 9, 980 (1961).

33. K. Shimizu, J. Phys. Soc. Japan 17, 508 (1962).

34. H. Warlimont, 5th Int. Cong. Electron Micros., Academic Press, N.Y., 1, p.HH-6.

35. G. R. Speich, to be published.

36. A. M. Turkalo, Trans. ASM 54, 344 (1961).

37. A. J. Lena, Precipitation from Solid Solution, ASM Cleveland, 1959, p.244.

38. R. F. Decker, J. T. Eash, and A. J. Goldman, Trans. ASM 55, 58 (1962).

39. A. H. Cottrell and B. A. Bilby, Proc. Phys. Soc. 62A, 49 (1949).

40. S. Harper, Phys. Rev. 83, 709 (1951).

41. W. Dahl and K. Lücke, Arch. Eisenhuttenw. 25, 241 (1954).

42. W. R. Thomas and G. M. Leake, J. Iron Steel Inst. 180, 155 (1955).

43. D. V. Wilson and B. Russell, Acta Met. 8, 468 (1960).

44. R. Bullough and R. C. Newman, Proc. Roy. Soc. 266, 209 (1962).

45. W. C. Leslie and A. S. Keh, J. Iron Steel Inst. 200, 722 (1962).

46. E. Nachtman and E. B. Moore, J. Metals 10, 281 (1958).

47. R. L. Rickett, S. H. Kalin and J. T. Mackenzie, Jr., Trans. AIME 185, 242 (1949).

48. W. C. Leslie, Ibid. 221, 752 (1961).

49. W. C. Leslie, J. T. Michalak and F. W. Aul, to be published, Metallurgical Soc. Conf. Volumes, John Wiley and Sons, N.Y.

50. E. Hornbogen, Trans. ASM 53, 569 (1961).

51. F. Garofalo, F. von Gemmingen and W. F. Domis, Ibid. 54, 430 (1961).

52. K. J. Irvine, J. D. Murray and F. B. Pickering, J. Iron Steel Inst. 196, 166 (1960).

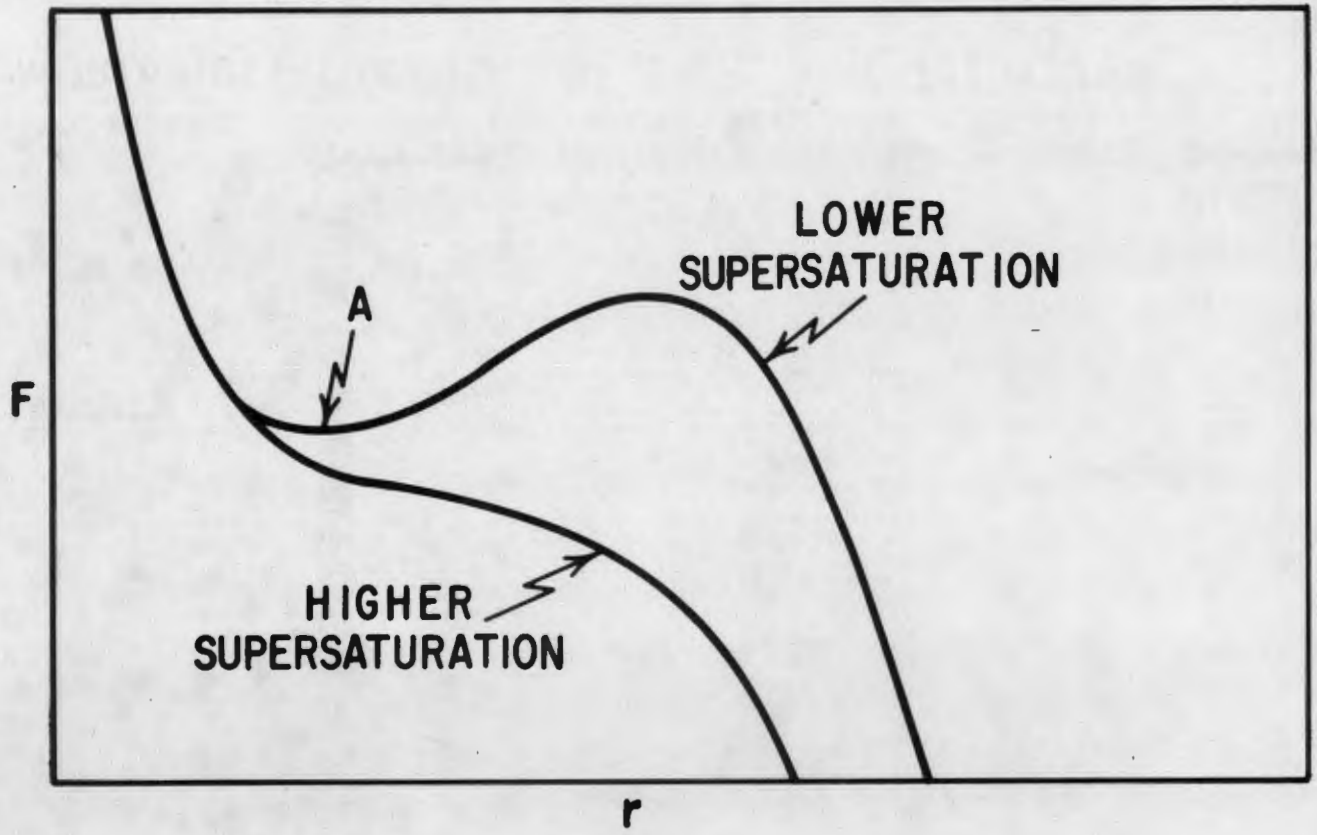

FIG. 1 -- FREE ENERGY PER UNIT LENGTH OF A CYLINDRICAL, NON-COHERENT NUCLEUS SURROUNDING A DISLOCATION[1].

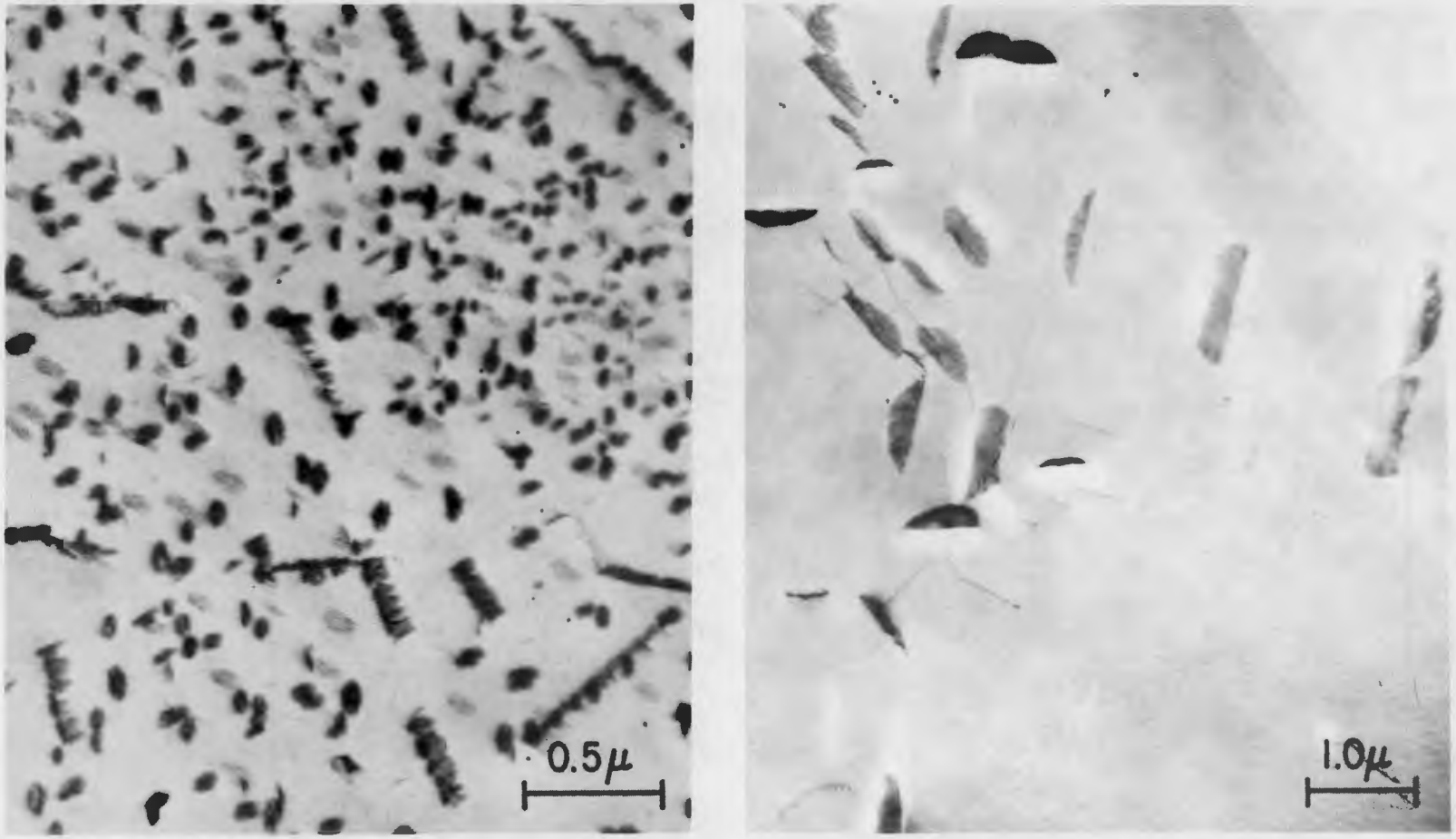

(a) 1 hr., 100°C, MATRIX PLUS DISLOCATION (b) 10 min., 200°C, DISLOCATION

FIG. 2 -- EFFECT OF AGING TEMPERATURE ON THE NUCLEATION OF $Fe_{16}N_2$ IN AN Fe-0.02% N ALLOY.

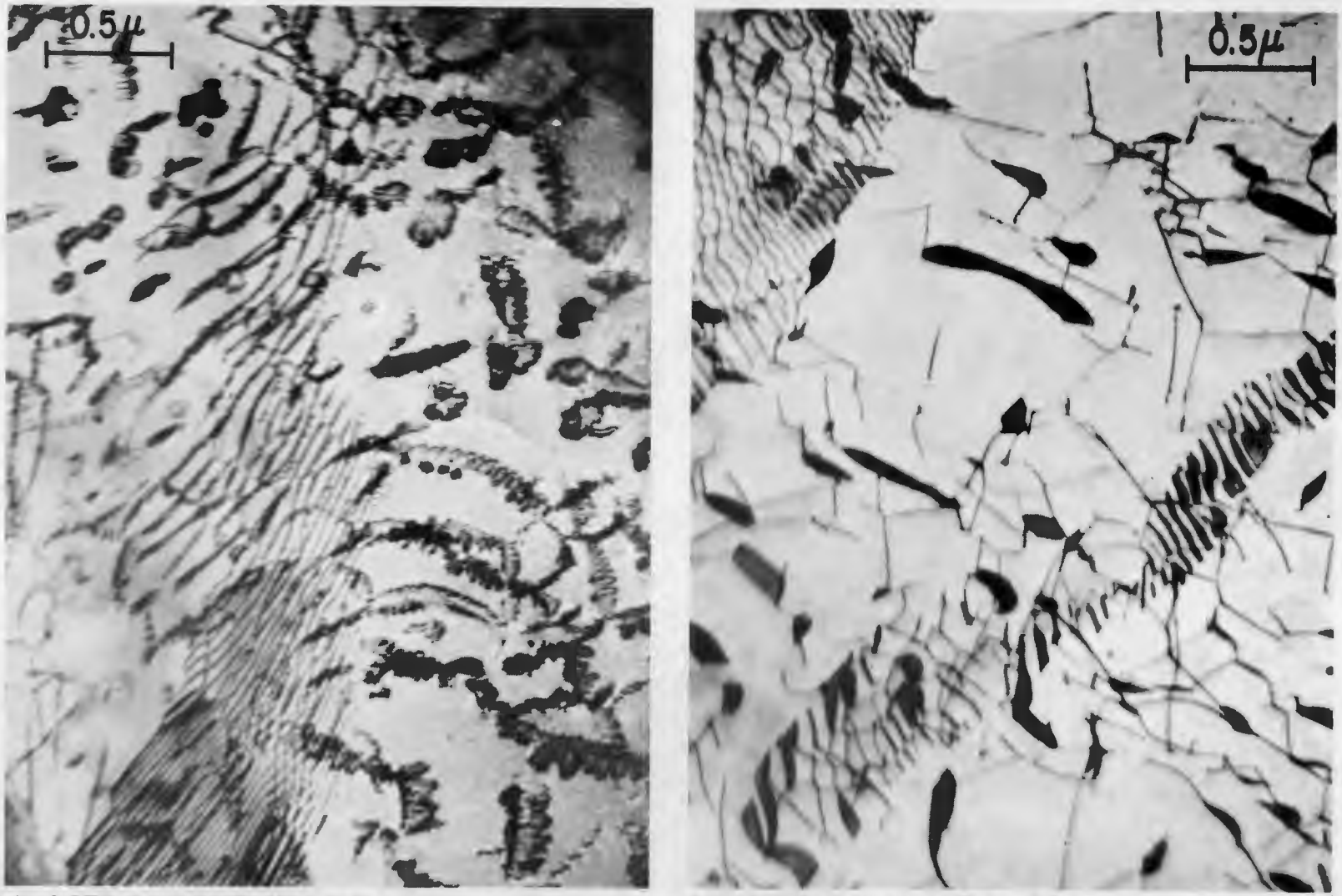

(a) AGED 26 DAYS AT 25°C

(b) AGED 2 MIN. AT 200°C

FIG. 3 -- PRECIPITATION OF $Fe_{16}N_2$ ON DISLOCATIONS AND SUBBOUNDARIES IN AN Fe-0.02% N ALLOY.

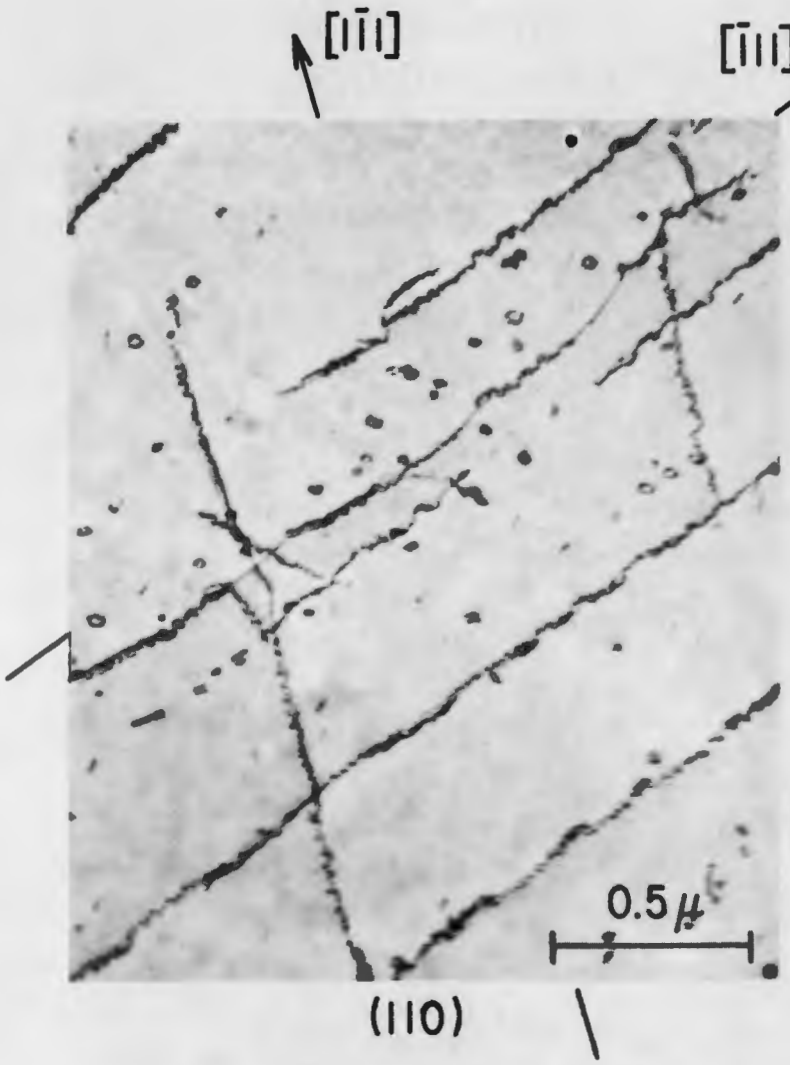

FIG. 4 -- PRECIPITATION OF CARBIDE ON SCREW DISLOCATIONS IN AN Fe-0.45Mn-0.017C ALLOY AGED 1 hr. AT 100°C.

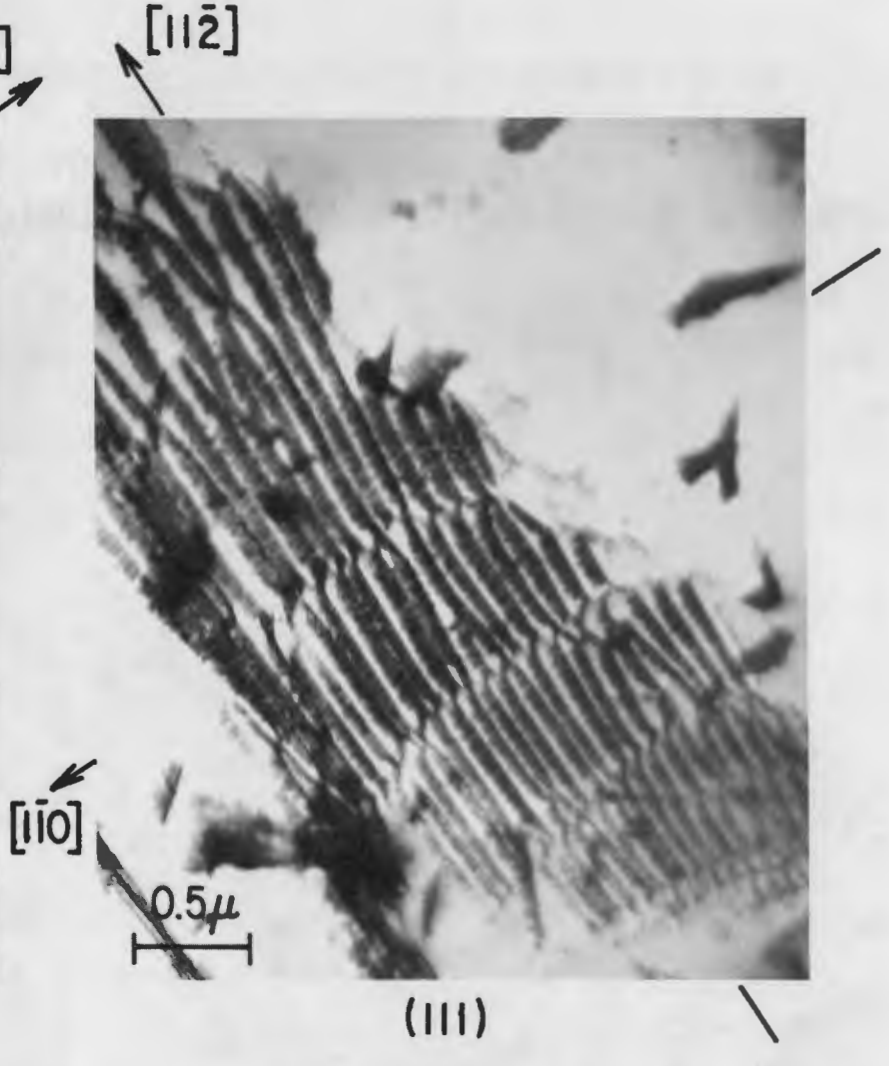

FIG. 5 -- PRECIPITATION OF $Fe_{16}N_2$ ON EDGE DISLOCATIONS IN A SIMPLE TILT BOUNDARY OF AN Fe-0.012%N ALLOY AGED 16 MONTHS AT 25°C.

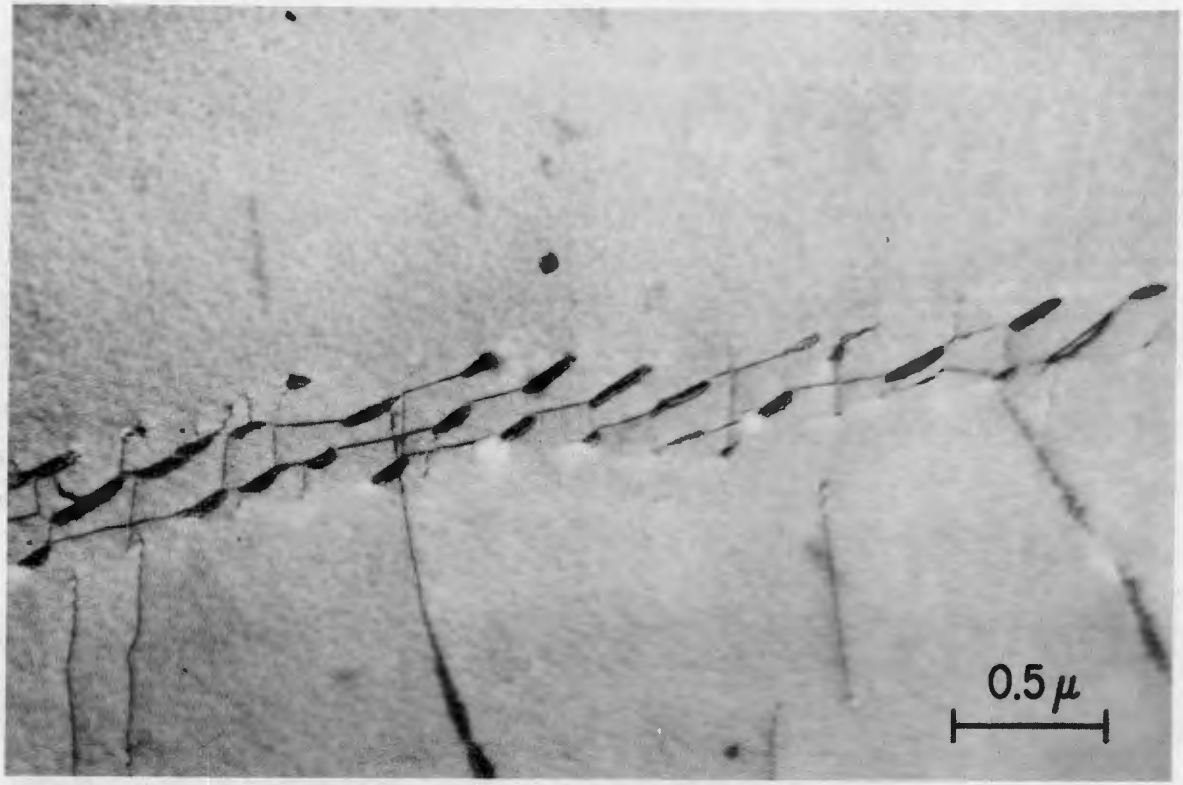

FIG. 6 -- CARBIDE PRECIPITATION ON A DISLOCATION NETWORK IN 3% SILICON STEEL AGED 256 HRS. AT 100°C.

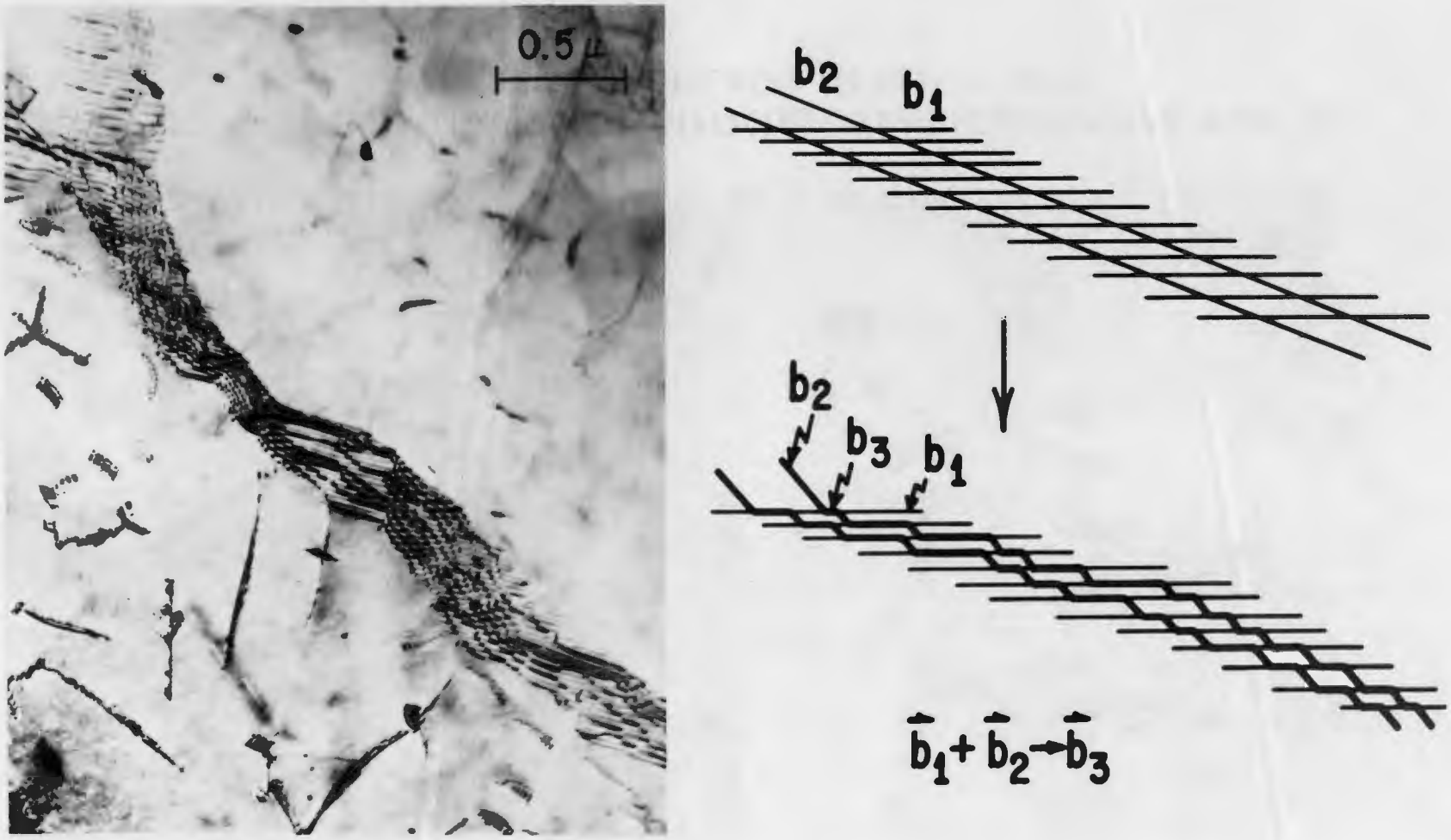

FIG. 7 -- PRECIPITATION OF $Fe_{16}N_2$ ON A SUBBOUNDARY IN AN Fe-0.01% N ALLOY AGED 2 HRS. AT 100°C.

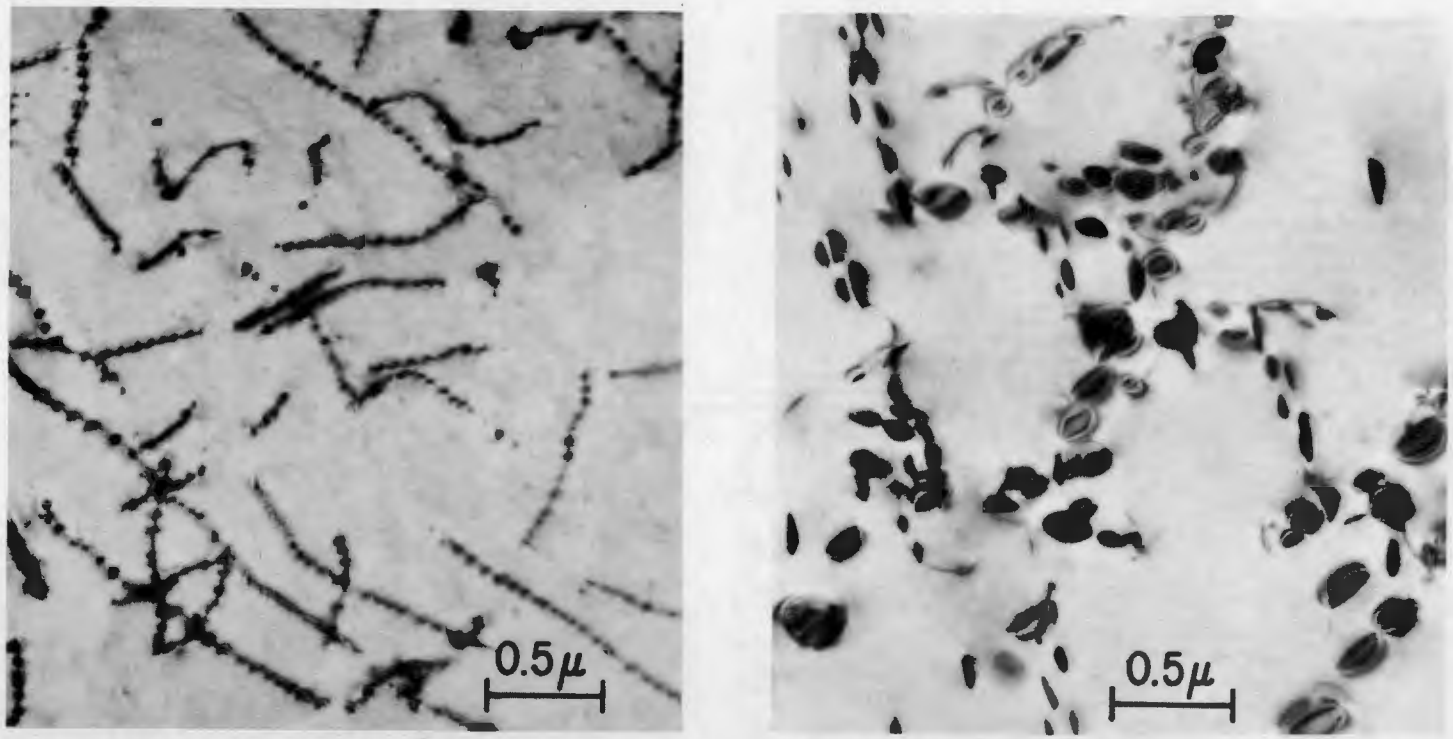

(a) 24 HRS. AT 500°C

(b) 6 HRS. AT 600°C

FIG. 8 -- NUCLEATION OF GOLD PARTICLES ON DISLOCATIONS IN A 1.1 at.% Au-Fe ALLOY.

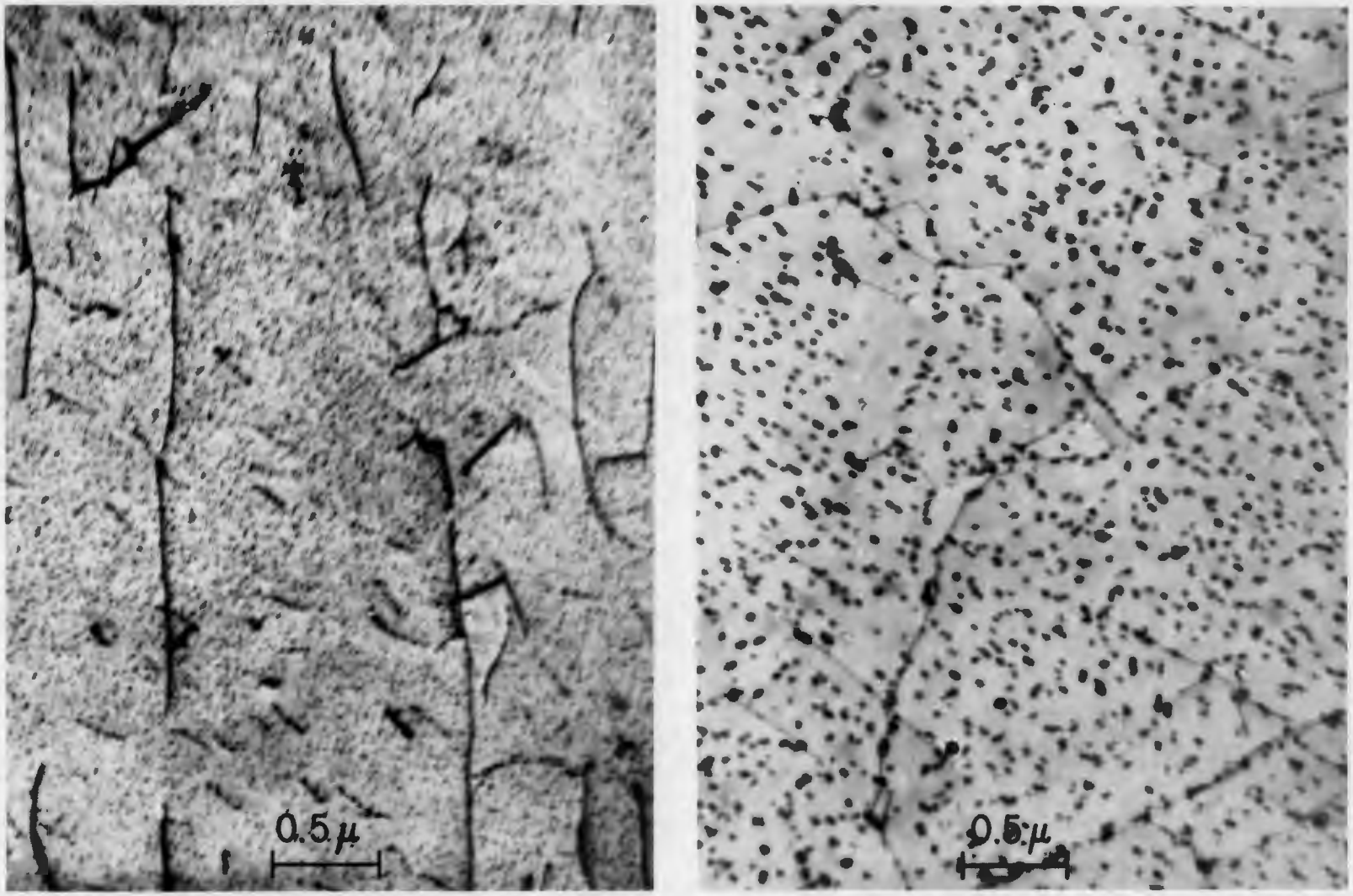

(a) 25 HRS. AT 500°C

(b) 100 HRS. AT 600°C

FIG. 9 -- PRECIPITATION OF COPPER PARTICLES IN FERRITE MATRIX IN A 1.08% Cu-Fe ALLOY.

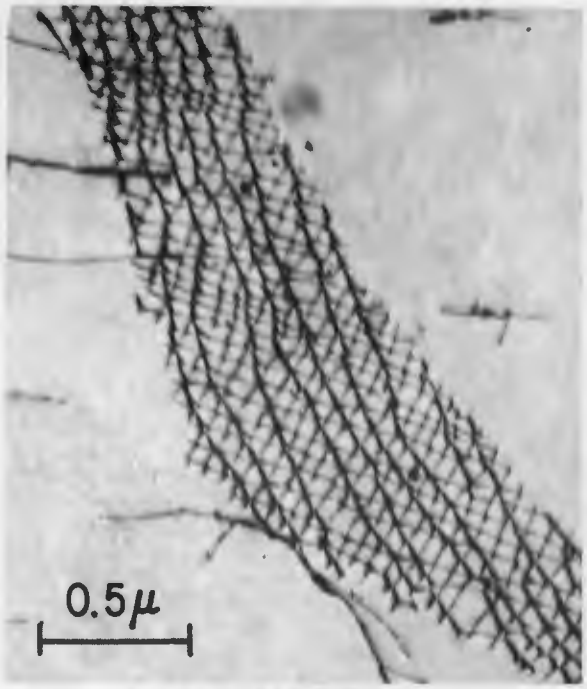

(a) AS QUENCHED

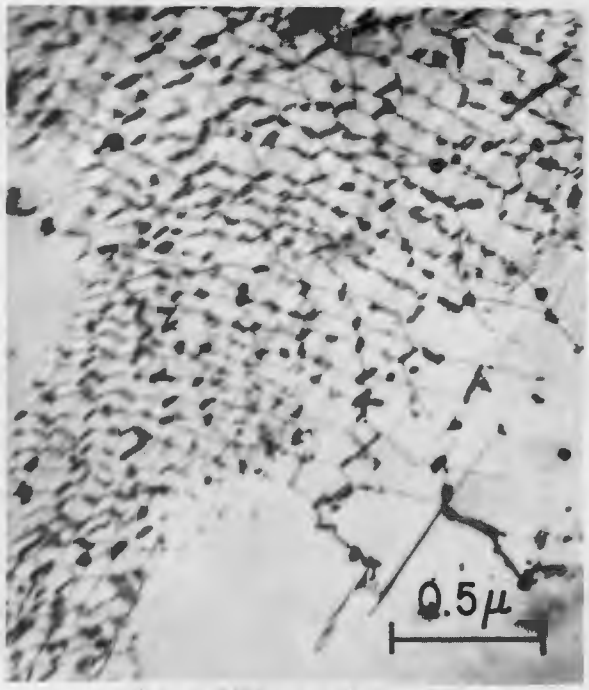

(b) AGED 4 HRS. AT 500°C

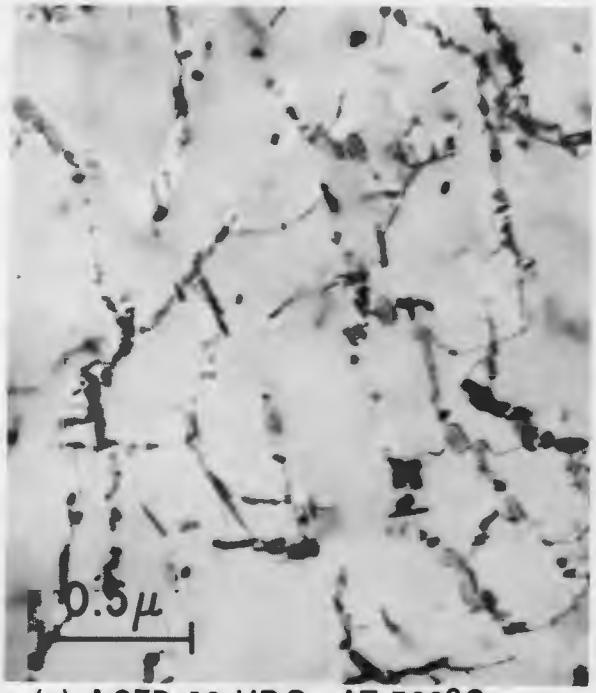

(c) AGED 10 HRS. AT 500°C

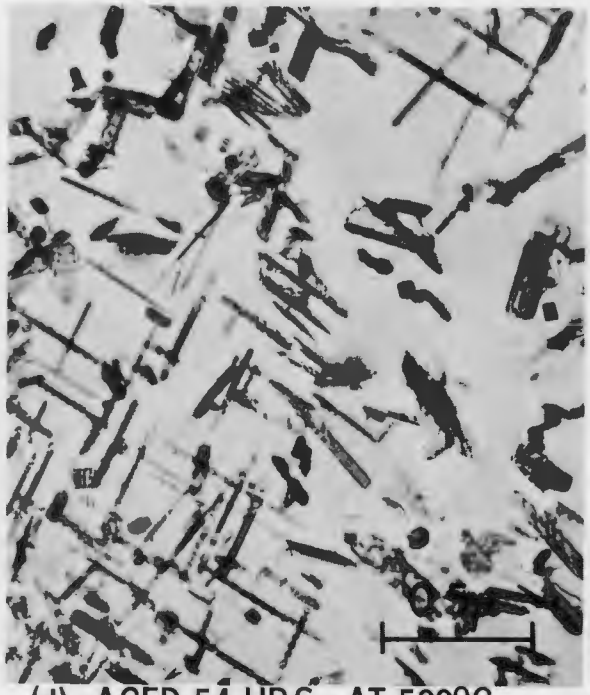

(d) AGED 54 HRS. AT 500°C

FIG. 10 -- PRECIPITATION IN AN Fe-1.8% P ALLOY, ROLLED 68% AT 1100°C, THEN QUENCHED.

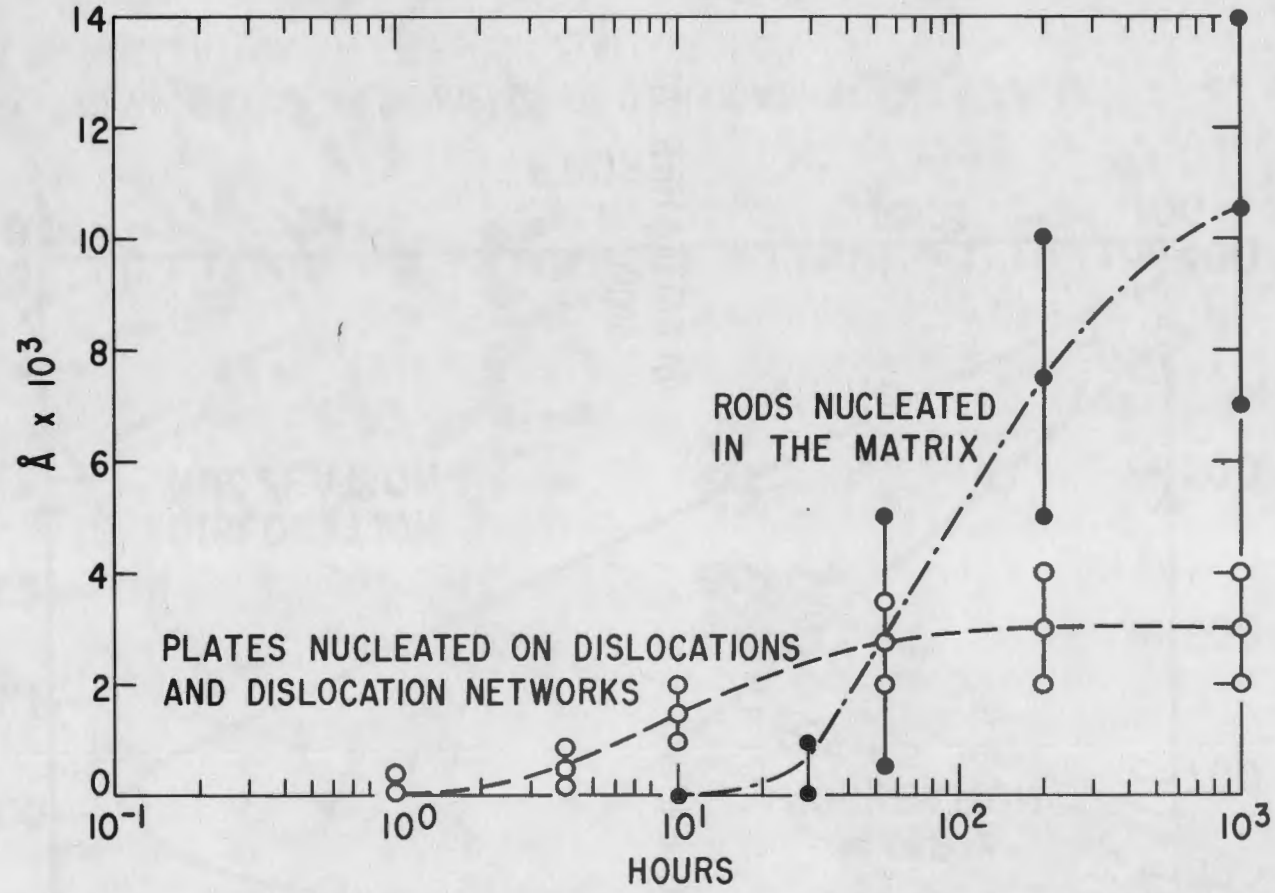

FIG. 11 -- GROWTH OF PHOSPHIDE PARTICLES AT DIFFERENT NUCLEATION SITES. Fe-1.8 wt.% P, QUENCHED FROM 1100°C AGED AT 500°C.

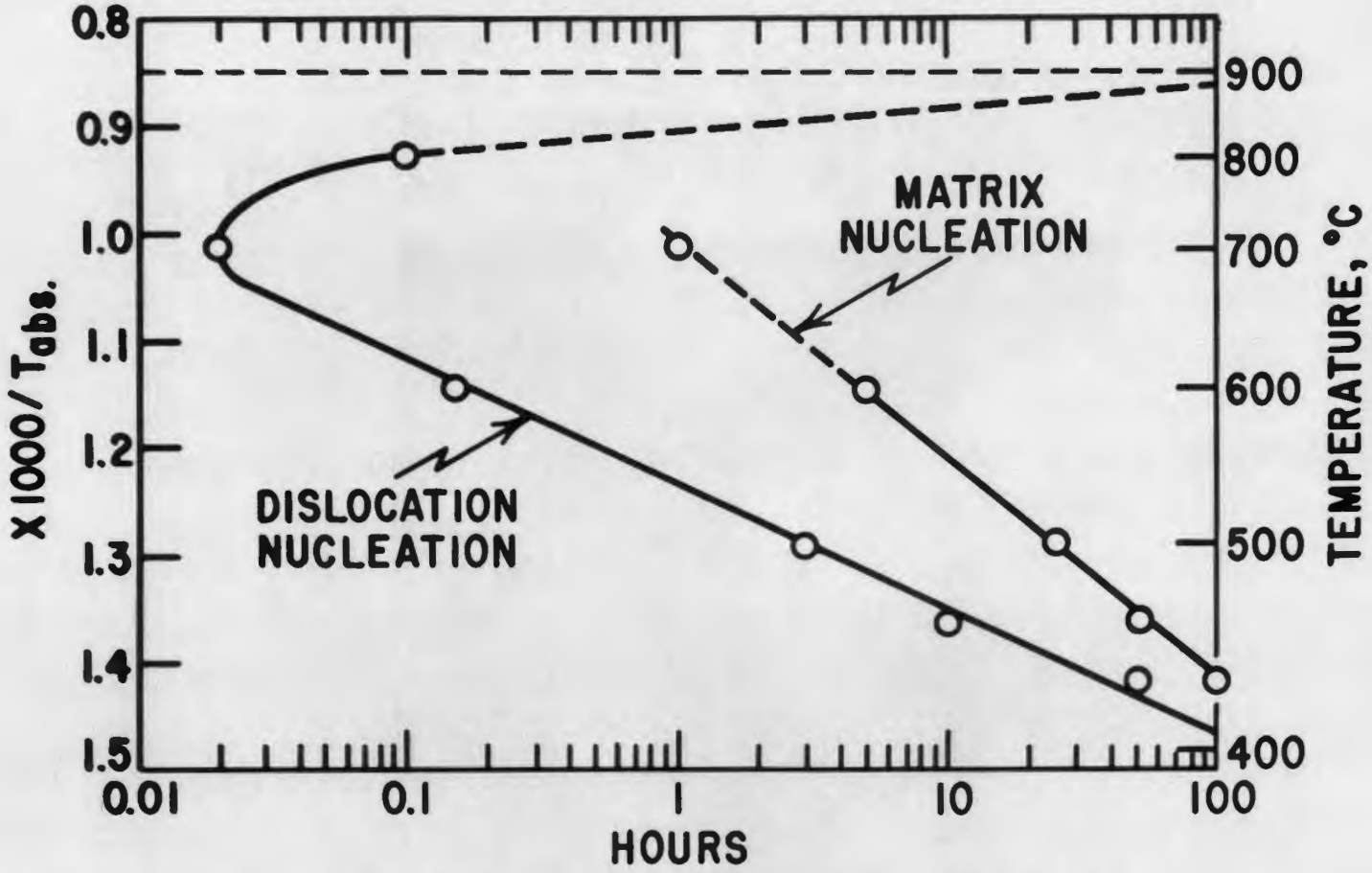

FIG. 12 -- TEMPERATURE DEPENDENCE OF DISLOCATION AND MATRIX NUCLEATION IN AN Fe-1.8% P ALLOY.

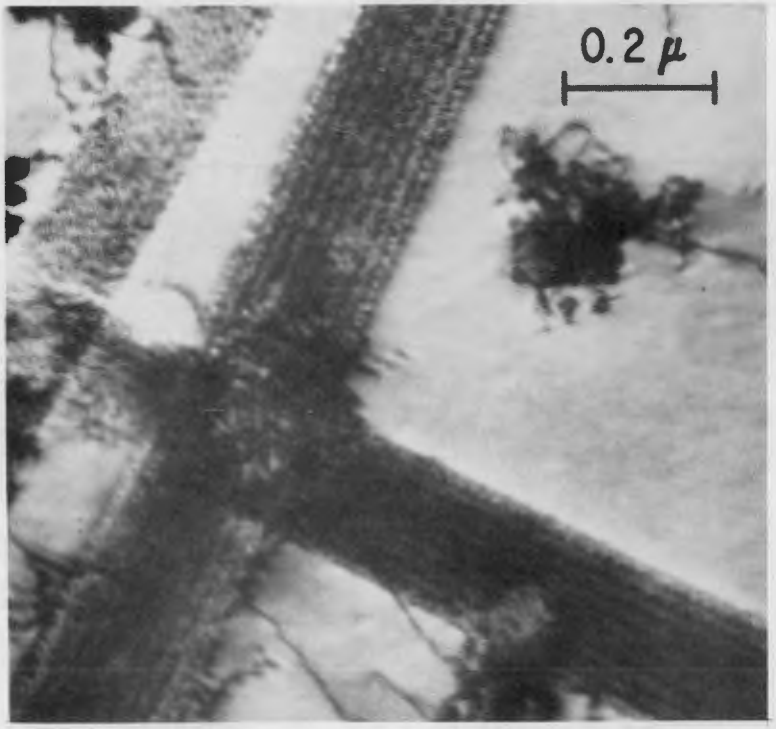

FIG. 13 -- PRECIPITATION ON STACKING FAULTS IN AN 18% Cr-10% Ni-1% Nb-0.1% C STAINLESS STEEL, TEMPERED 72 HRS. AT 700°C. (AFTER VAN ASWEGEN AND HONEYCOMBE [28])

FIG. 14 -- INTERNAL TWINNED STRUCTURE OF MARTENSITE PLATES IN A QUENCHED 1.0% C STEEL. (KELLY AND NUTTING[30])

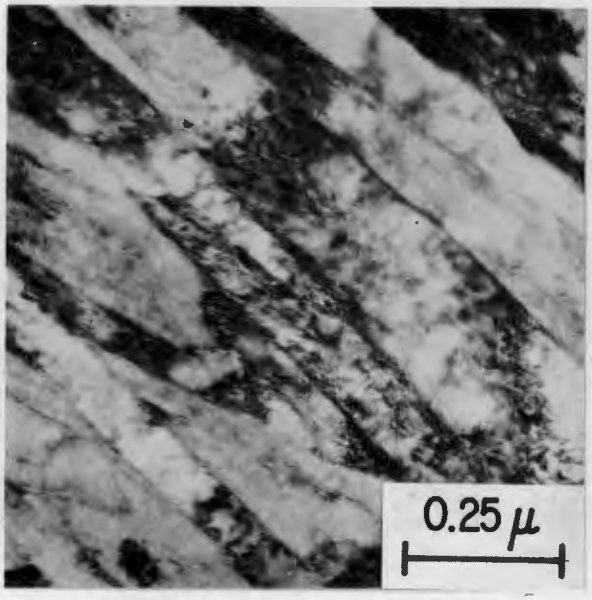

FIG. 15 -- MARTENSITE NEEDLES WITH NO INTERNAL TWINNING BUT HIGH DISLOCATION DENSITY FORMED IN A 0.1% C STEEL. (KELLY AND NUTTING[30])

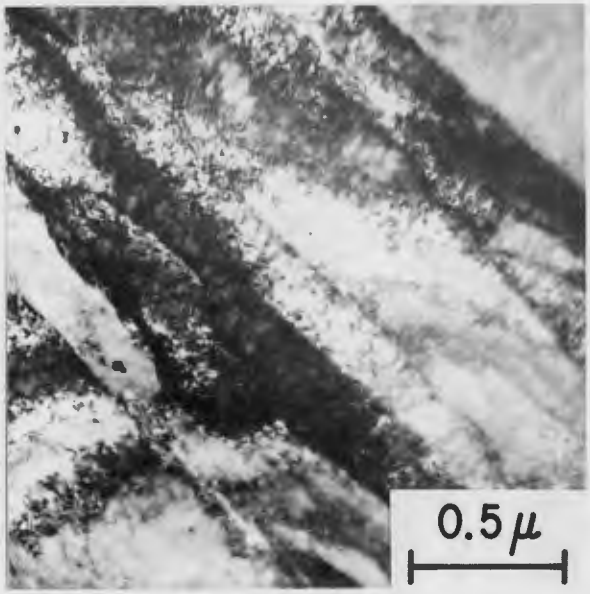

FIG. 16 -- STRUCTURE OF MARTENSITE IN AN Fe-20 Ni ALLOY.

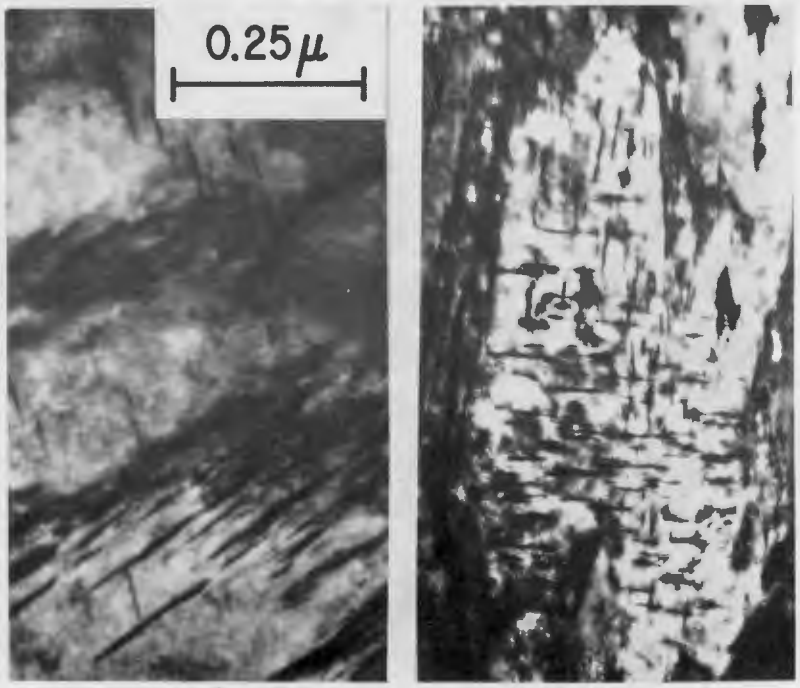

FIG. 17 -- CARBIDES FORMED IN A 0.42% C STEEL TEMPERED AT 600°F (315°C) (a) "STREAKY CARBIDES", (b) "CRYSTALLOGRAPHIC CARBIDES" (TURKALO[36])

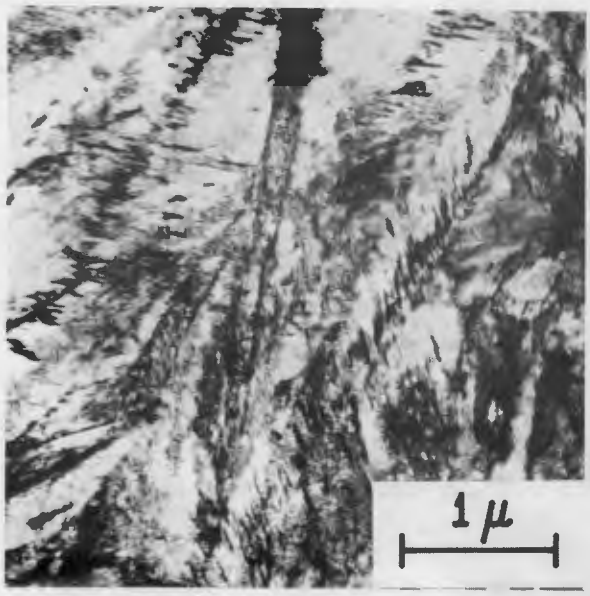

FIG. 18 -- 1.0% C STEEL TEMPERED FOR 1 HR. AT 300°C (KELLY AND NUTTING[31])

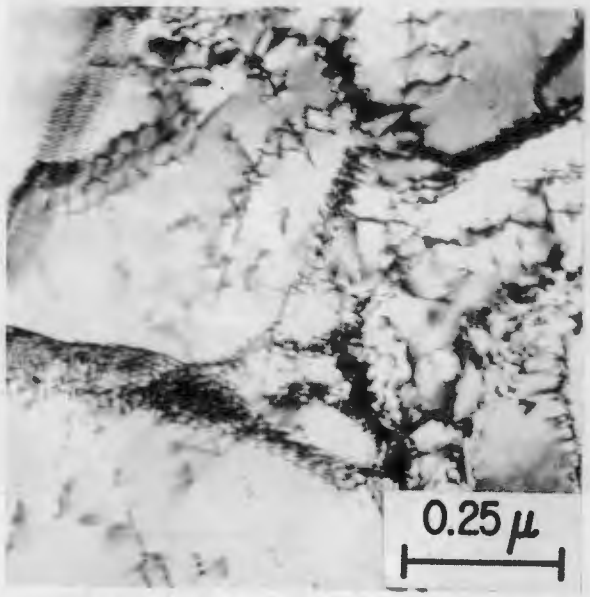

FIG. 19 -- POLYGONIZED SUBSTRUCTURE FORMED BY RECOVERY OF TRANSFORMATION SUBSTRUCTURE IN AN Fe-18 Ni-7 Co ALLOY AGED AT 500°C FOR 100 HRS.

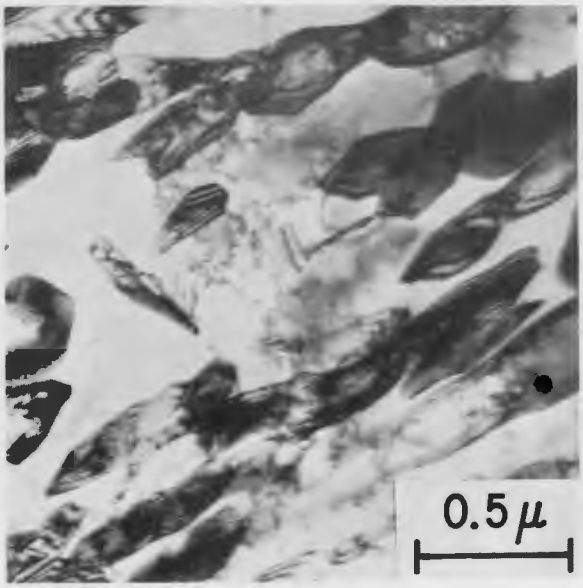

FIG. 20 -- FORMATION OF AUSTENITE IN AN Fe-20Ni ALLOY AFTER AGING AT 500°C FOR 100 HRS.

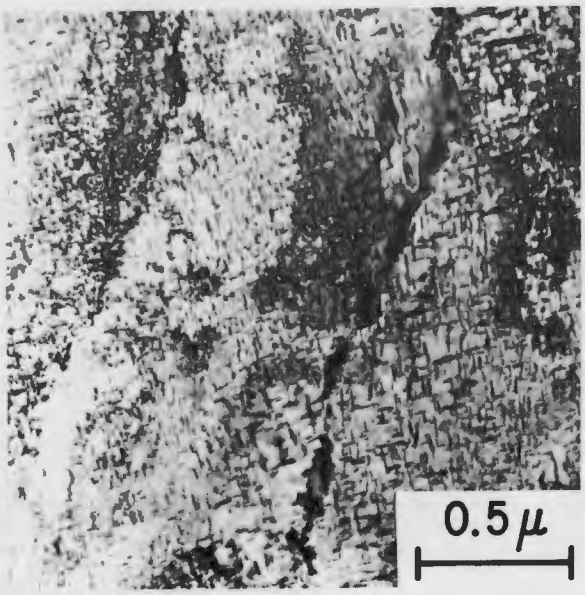

FIG. 21 -- PRECIPITATION IN A MARTENSITIC Fe-20Ni-1Ti ALLOY AGED AT 500°C FOR 24 HRS.

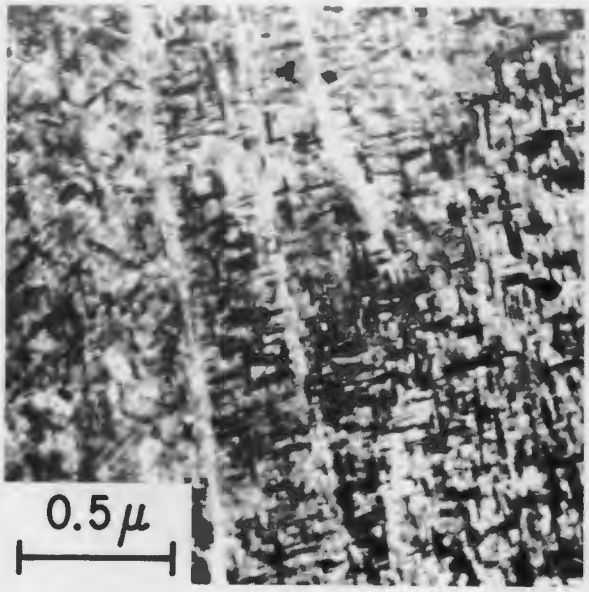

FIG. 22 -- PRECIPITATION IN A MARTENSITIC Fe-20 Ni-10 Cu ALLOY AGED AT 500°C FOR 100 HRS.

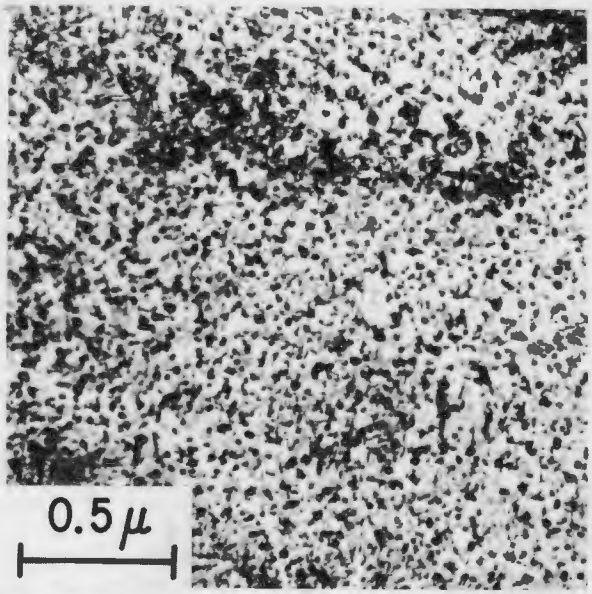

FIG. 23 -- PRECIPITATION IN A MARTENSITIC Fe-18 Ni-7 Co-5 Mo ALLOY AGED AT 500°C FOR 8 HRS.

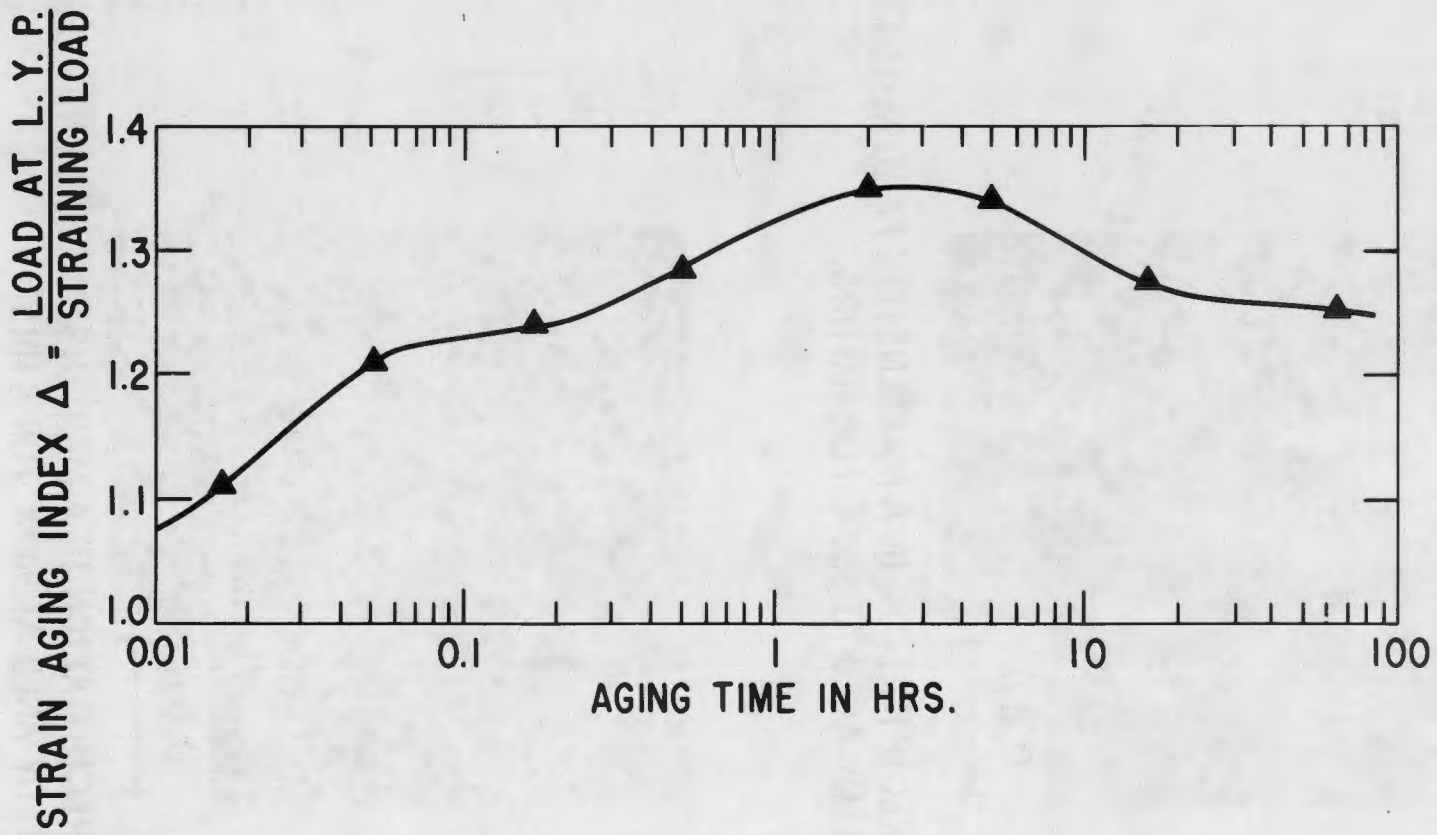

FIG. 24 -- STRAIN AGING OF A 0.022% N ALLOY, QUENCHED FROM 500°C, STRAINED 3%, AGED AT 100°C.

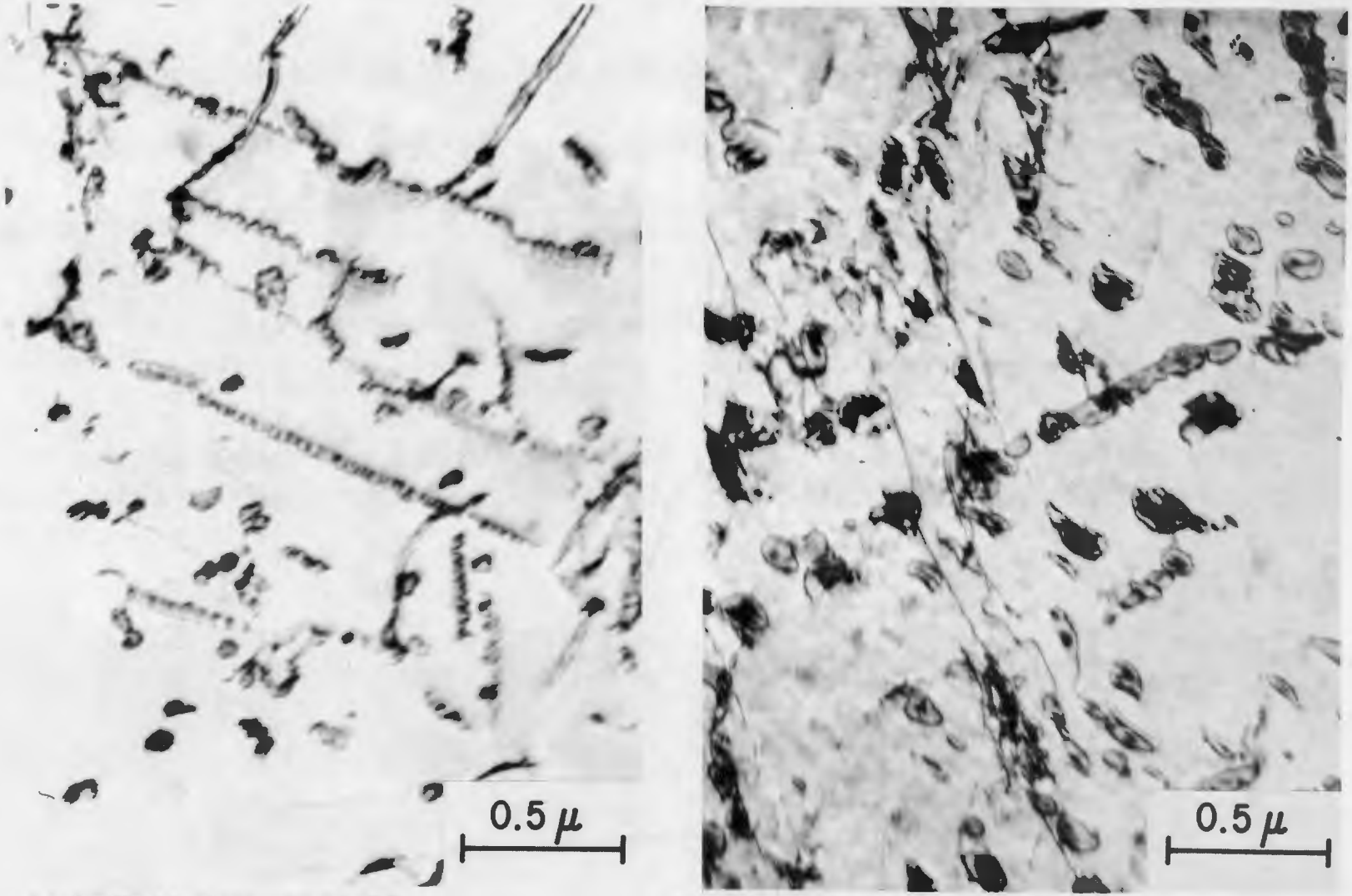

(a) AGED 30 MIN. AT 100°C

(b) AGED 16 HRS. AT 100°C

FIG. 25 -- NITRIDE PRECIPITATION AFTER STRAIN AGING OF A QUENCHED 0.022% N ALLOY, STRAINED 3%.

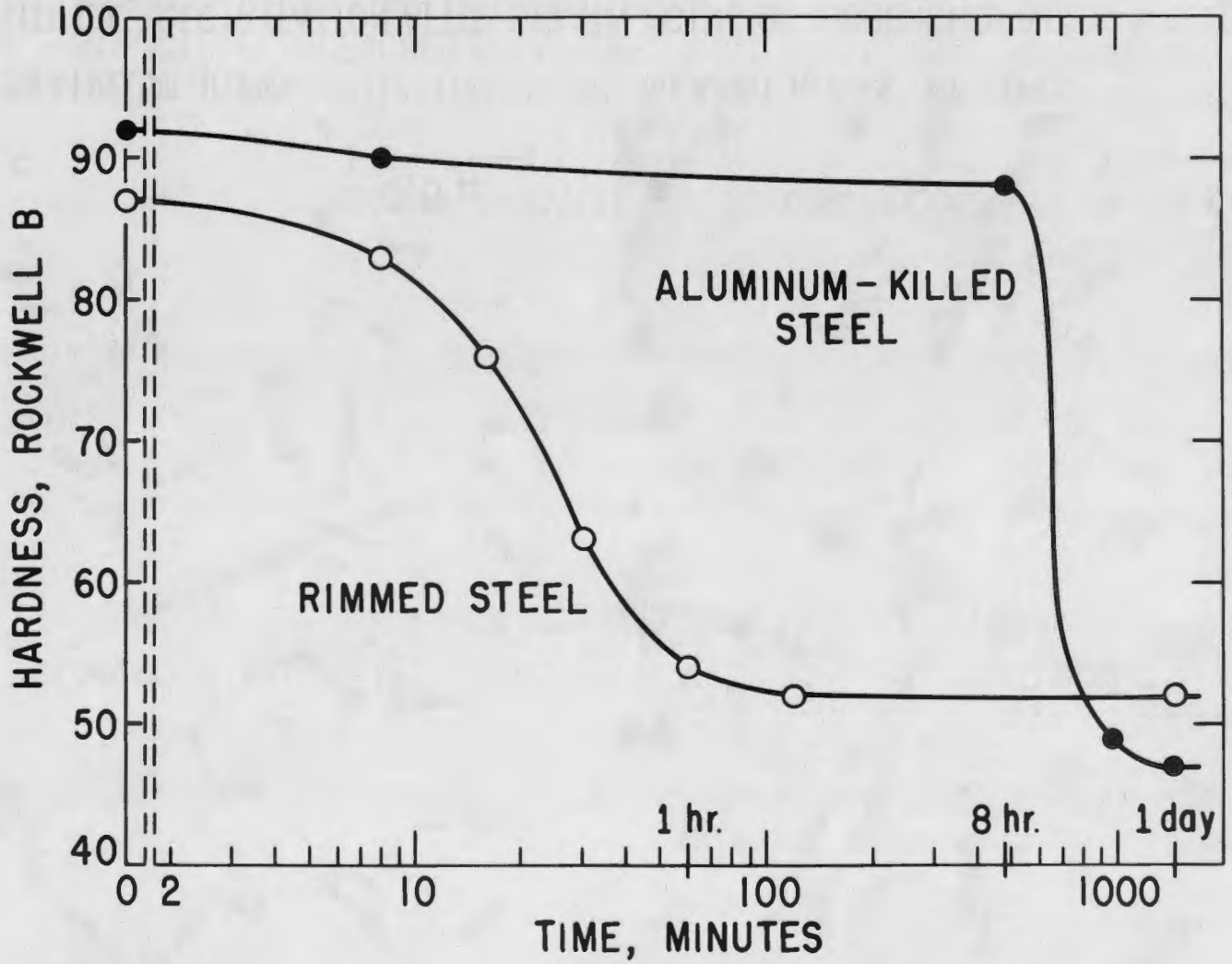

FIG. 26 -- RECRYSTALLIZATION OF LOW-CARBON SHEET STEEL AT 565°C, AFTER 40% COLD REDUCTION.

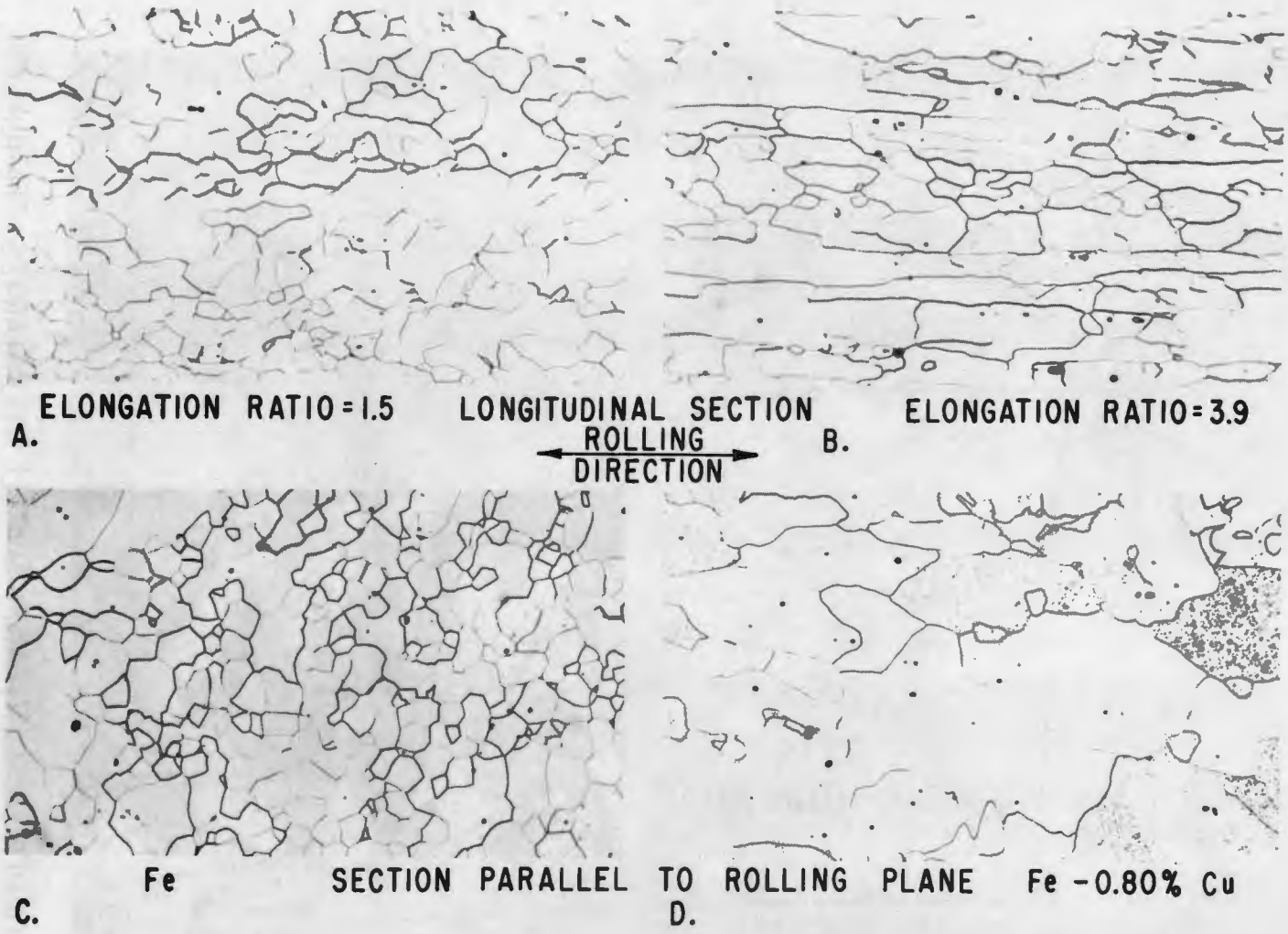

FIG. 27 -- EFFECT OF PRECIPITATION BEFORE RECRYSTALLIZATION ON FERRITE GRAIN STRUCTURE. (QUENCHED FROM 925°C, COLD ROLLED 90%, PRETREATED 3 HRS. AT 500°C, RECRYSTALLIZED AT 700°C)
200X NITAL ETCH

FIG. 28 -- COPPER PRECIPITATED IN CELL BOUNDARIES. Fe-0.8% Cu, COLD ROLLED 60%, HELD 3 HRS. AT 500°C, 10 MIN. AT 650°C.

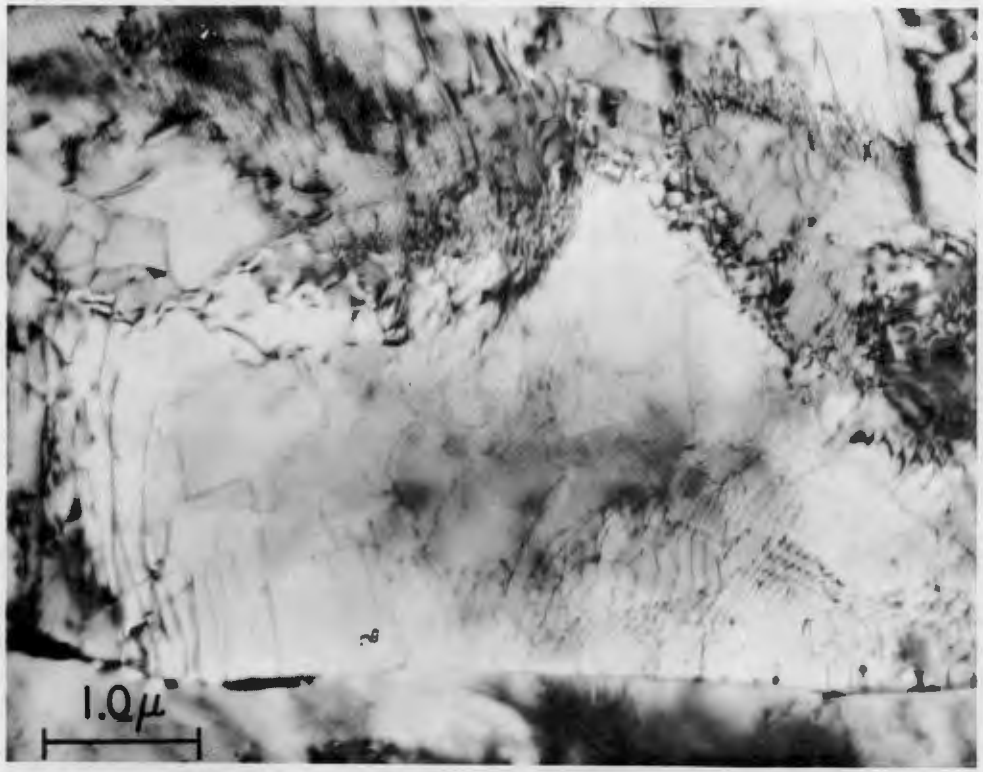

FIG. 29 -- COPPER PRECIPITATED IN GRAIN BOUNDARY DURING TREATMENT AT 500°C PRIOR TO RECRYSTALLIZATION. Fe-0.8% Cu, QUENCHED FROM 925°C, C. R. 60%, HELD 3 HRS. AT 500°C.

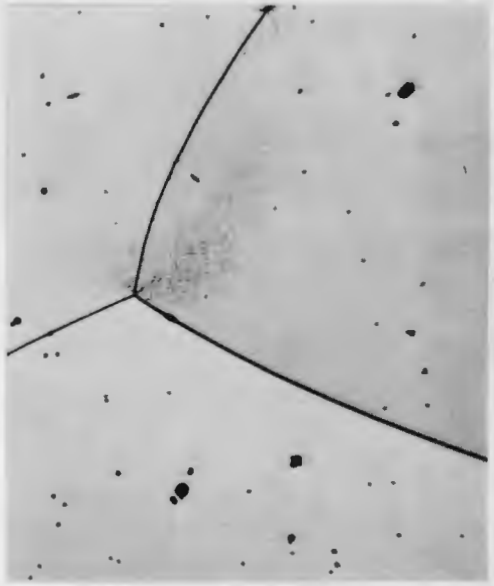

(a) AS QUENCHED WITHOUT ROLLING, DISLOCATION DENSITY = $10^8/cm^2$.

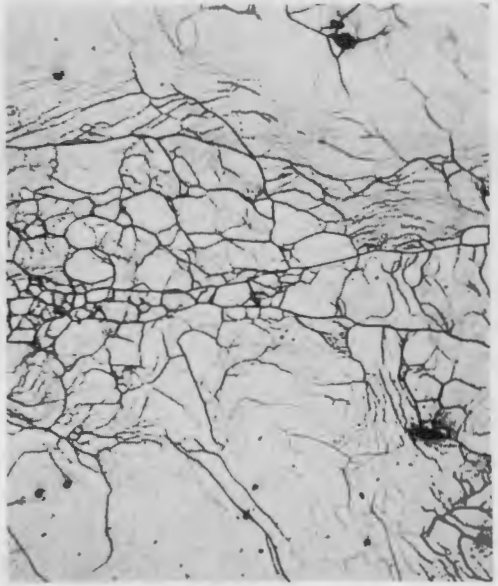

(b) ROLLED 40% AT 1100°C DISLOCATION DENSITY = $1 \times 10^{10}/cm^2$.

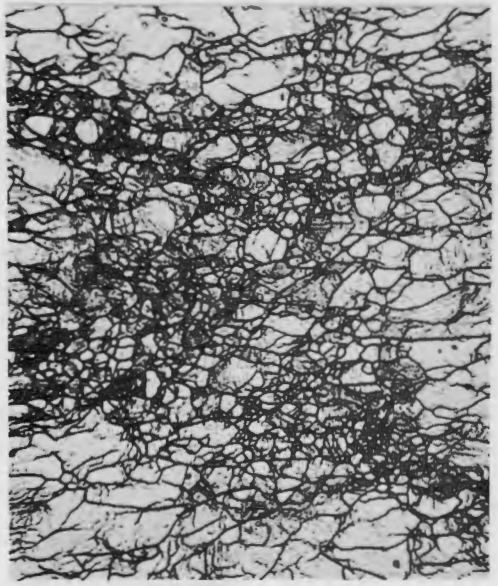

(c) ROLLED 68% AT 1100°C DISLOCATION DENSITY = $5 \times 10^{10}/cm^2$.

FIG. 30 -- DISLOCATION STRUCTURES IN AN Fe-1.8%P ALLOY, QUENCHED FROM 1100°C AFTER ROLLING, THEN AGED 8 HRS. AT 500°C. 500X

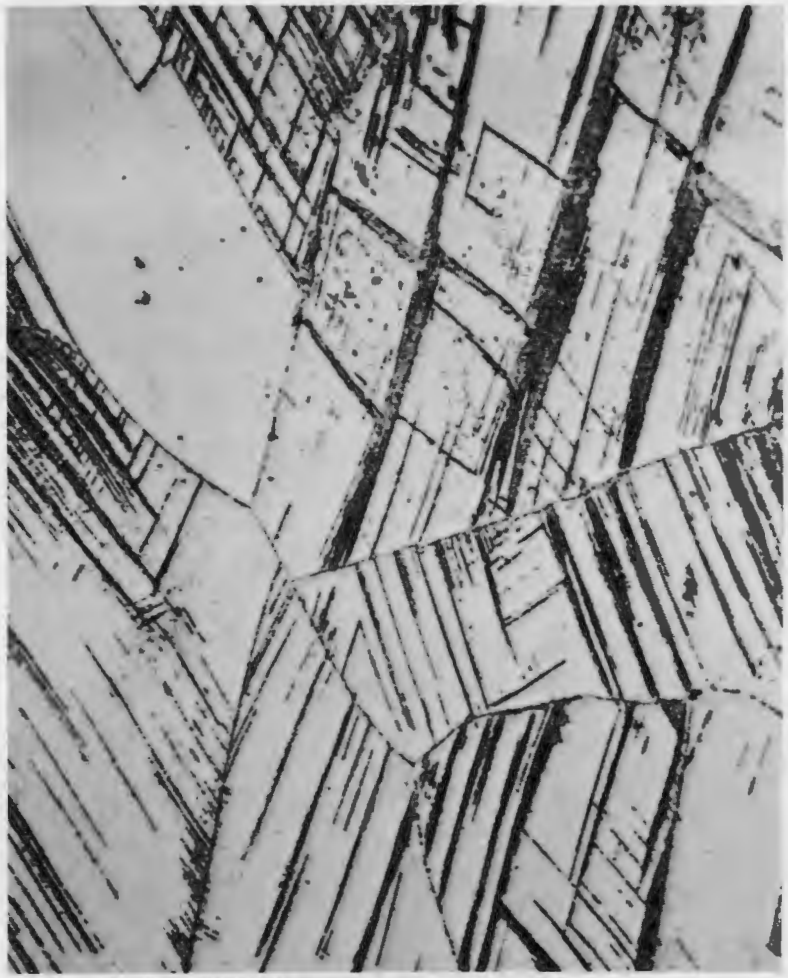

(a) LIGHT MICROGRAPH, 1000X

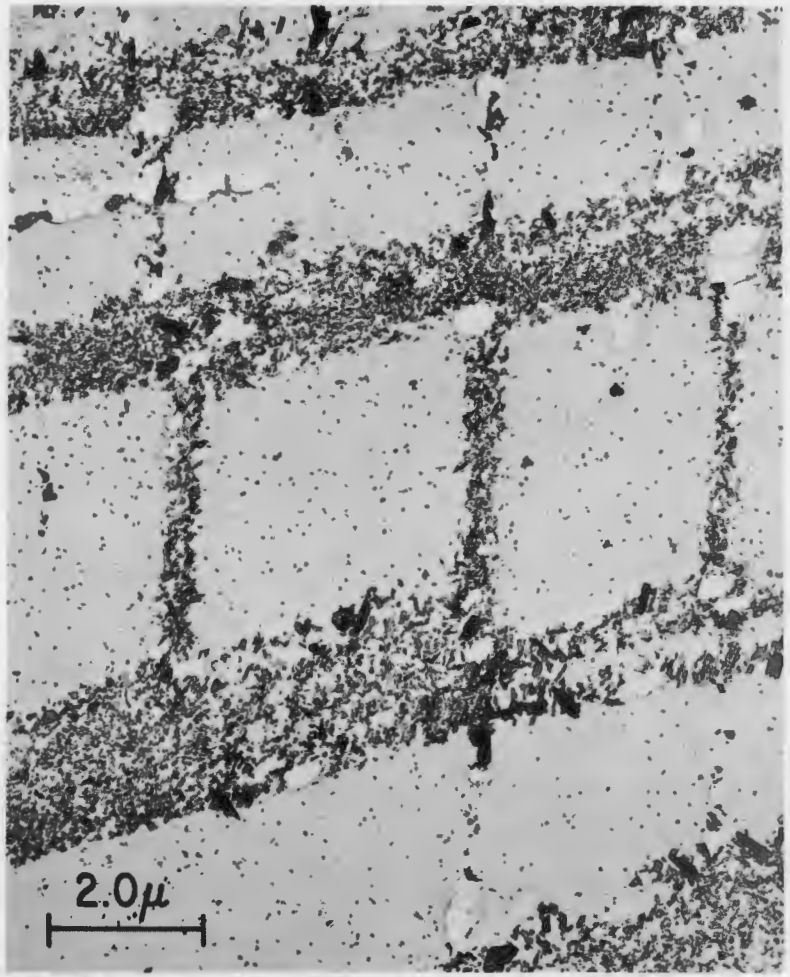

(b) EXTRACTION REPLICA

FIG. 31 -- STRUCTURE OF TYPE 316 STAINLESS STEEL QUENCHED FROM 1095°C STRAINED 25%, AGED AT 480°C AND AT 705°C, THEN CREEP TESTED AT 705°C.